Slip Heating in Polymer Processing

By

Peter H Gilbert

A thesis submitted to the Graduate Program in Chemical Engineering
in conformity with the requirements for the
Degree of Master of Applied Science

Queen's University
Kingston, Ontario, Canada
December 2014

Abstract

When one body slips on another, heat is generated at the slipping interface. We call this phenomenon *slip heating* and apply slip heating theory to cohesive and adhesive slip in extrusion dies. Adhesive slip, which is linked to *melt fracture*, is a breakdown of the no slip boundary condition at the die wall, where the fluid moves with respect to the wall. *Die drool*, the accumulation of plastic on the open die face, has been attributed to cohesive melt failure, which results in the formation of a *bulk layer* that slips on a *drool layer*. The corresponding isothermal analysis of cohesive slip led to an analytical solution for the drool rate [Schmalzer and Giacomin, *J. Pol. Eng.*, **33**, 1 (2013)]. We account for slip heating during adhesive and cohesive slip and develop analytical solutions for temperature rise with and without viscous dissipation. We focus on slit flow, used in film casting, sheet extrusion and curtain coating, and when curvature can be neglected, slit flow is easily extended to pipe extrusion and film blowing. In slit flow, the heat flux from the slipping interface is the product of the shear stress and the slip speed. We present the solutions for the temperature rise in pressure-driven and simple shearing flows, each subject to constant heat generation at the slipping interface. We find expressions for drool rate by modeling viscosity as an Arrhenius function of temperature, and we show how to correct wall slip data for the slip heating temperature rise. We conclude with worked examples showing the importance of slip heating in die drool and wall slip, and we find that slip heating suppresses drool. We also arrive at a necessary dimensionless condition for the accurate use of our results: $\text{Pé} \ll 1$.

Acknowledgment

This research was undertaken, in part, thanks to funding from the Canada Research Chairs program of the Government of Canada of the Tier 1 Canada Research Chair in Rheology. A. J. Giacomin is indebted to the Faculty of Applied Science and Engineering of Queen's University at Kingston, for their support through a Research Initiation Grant (RIG). We are grateful for the valuable input of Dr. A.M. Schmalzer of the Los Alamos National Laboratory (formerly with the University of Wisconsin-Madison) in developing slip heating theory. We thank The Society of Rheology for the opportunity to present this work at their 86th annual meeting in Philadelphia, PA [1]. For a corresponding travel grant, we thank the Chemical Engineering Department of Queen's University.

CONTENTS

List of Tables

List of Figures

Table 1: Dimensional Variables

Name	Symbol	Dimensions	Range
Absolute pressure	p	$ML^{-1}t^{-2}$	≥ 0
Absolute temperature	T	T	≥ 0
Absolute temperature, bulk fluid	T_b	T	≥ 0
Absolute temperature, drool layer	T_d	T	≥ 0
Absolute temperature, fluid	T_f	T	≥ 0
Absolute temperature, initial	T_0	T	≥ 0
Absolute temperature, interface at steady state	$T_{i,\infty}$	T	≥ 0
Absolute Temperature, melt degradation	T_D	T	≥ 0
Absolute temperature, reference	T_r	T	≥ 0
Absolute temperature, slip interface	T_i	T	≥ 0
Absolute temperature, wall	T_m	T	≥ 0
Absolute temperature, wall exterior	T_w	T	≥ 0
Acceleration of gravity	g	Lt^{-2}	≥ 0
Area (normal vector)	$\vec{A}$	L^2	≥ 0
Arrhenius exponential constant	B	T	≥ 0
Bulk fluid thickness	$2b$	L	≥ 0
Characteristic length [see Eq. (124)]	$\Xi \equiv \frac{\tau_c L}{\Delta p}$	L	≤ 0
Cohesive/Critical fracture strength	τ_c	$ML^{-1}t^{-2}$	≥ 0
Density	ρ	ML^{-3}	≥ 0
Density: fluid, wall	ρ_f, ρ_m	ML^{-3}	≥ 0
Die gap (cohesive)/ Total die thickness: gap + walls (adhesive)	h	L	≥ 0
Displacement (vector)	$\vec{d}$	L	$\mathbb{R}^3$
Distance from die entrance or end of sample	y	L	≥ 0
Distance from slip interface	x	L	$-d \leq x \leq b$
Drool layer (Cohesive)/ Wall thickness (Adhesive)	d	L	≥ 0

Extra stress tensor[1]	$\boldsymbol{\tau}$	$ML^{-1}t^{-2}$	$\mathbb{R}^3$
Force (vector)	$\vec{F}$	MLt^{-2}	$\mathbb{R}^3$
Heat capacity, isobaric	$\hat{C}_p$	$L^2t^{-2}T^{-1}$	≥ 0
Heat capacity, isobaric: fluid, wall	$\hat{C}_{p,f}, \hat{C}_{p,m}$	$L^2t^{-2}T^{-1}$	≥ 0
Heat flux vector	$\vec{q}$	Mt^{-3}	$\mathbb{R}$
Interfacial heat flux	$q_i \equiv q_x\big\vert_{x=0} = u_s\tau_c$	Mt^{-3}	≥ 0
Interfacial slip speed	u_s	Lt^{-1}	≥ 0
Power	$\dot{Q}$	ML^2t^{-3}	$\mathbb{R}$
Sample or slit length	L	L	≥ 0
Shear stress[1]	τ_{ij}	$ML^{-1}t^{-2}$	≥ 0
Slip activation energy	E_s	T	$\mathbb{R}$
Slit pressure drop	ΔP	$ML^{-1}t^{-2}$	≤ 0
Slit width	w	L	≥ 0
Temperature change, slip heating	ΔT_{SH}	T	≥ 0
Temperature change, slip heating + viscous dissipation	ΔT_{SHVD}	T	≥ 0
Thermal conductivity	k	$MLt^{-3}T^{-1}$	≥ 0
Thermal conductivity: fluid, wall	k_f, k_m	$MLt^{-3}T^{-1}$	≥ 0
Thermal diffusivity	α	L^2t^{-1}	≥ 0
Thermal diffusivity: fluid, wall	α_f, α_m	L^2t^{-1}	≥ 0
Time	t	t	≥ 0
Velocity gradient tensor	∇v	t^{-1}	$\mathbb{R}^3$
Velocity, along die length	v_y	Lt^{-1}	≥ 0
Velocity, bulk	v_b	Lt^{-1}	≥ 0
Velocity, drool	v_d	Lt^{-1}	≥ 0
Velocity, fluid	v_f	Lt^{-1}	≥ 0
Velocity, maximum	v_{max}	Lt^{-1}	≥ 0
Velocity, wall	v_w	Lt^{-1}	≥ 0
Viscosity	μ	$ML^{-1}t^{-1}$	≥ 0
Viscosity at Wall temperature	μ_w	$ML^{-1}t^{-1}$	≥ 0
Volumetric flow rate, bulk	$\dot{V}_b$	L^3t^{-1}	≥ 0

[1] Where τ_{ij} is the force exerted in the *j*th direction on a unit area of fluid surface of constant x_i by fluid in the region lesser x_i on fluid in the region greater x_i [24].

Volumetric flow rate, drool	$\dot{V}_d$	L^3t^{-1}	≥ 0
Work by wall on fluid	$\tilde{W}$	ML^2t^{-2}	$\mathbb{R}$

Legend: $M \equiv$ mass; $L \equiv$ length; $t \equiv$ time; $T \equiv$ temperature

Table 2: Dimensionless Variables

Name	Symbol	Range
Absolute temperature	$\Theta = \frac{T - T_0}{T_0}$	≥ 0
Absolute temperature, bulk fluid	$\Theta_b = \frac{T_b - T_0}{T_0}$	≥ 0
Absolute temperature, drool layer	$\Theta_d = \frac{T_d - T_0}{T_0}$	≥ 0
Absolute temperature, fluid	$\Theta_f = \frac{T_f - T_0}{T_0}$	≥ 0
Absolute temperature, interface	$\Theta_i = \frac{T_i - T_0}{T_0}$	≥ 0
Absolute temperature, interface at steady state	$\Theta_{i,\infty} = \frac{T_{i,\infty} - T_0}{T_0}$	≥ 0
Absolute temperature, maximum	$\Theta_{max} = \frac{T_{max} - T_0}{T_0}$	≥ 0
Absolute Temperature, melt degradation	$\Theta_D = \frac{T_D - T_0}{T_0}$	≥ 0
Absolute temperature, wall exterior	$\Theta_w = \frac{T_w - T_0}{T_0}$	≥ 0
Absolute temperature, wall layer	$\Theta_m = \frac{T_m - T_0}{T_0}$	≥ 0
Arrhenius exponential constant, thermal sensitivity	$\beta = \frac{B}{T_{i,\infty}}$	≥ 0
Arrhenius shift factor	$a_{T,s}$	≥ 0
Brinkman Number, pressure-driven flow	$\mathrm{Br} \equiv \frac{\mu}{kT_0}\left(\frac{b^2 \Delta P}{L\mu}\right)^2$	≥ 0
Brinkman Number, simple shear flow	$\mathrm{Br} \equiv \frac{\mu v_w^2}{kT_0}$	≥ 0
Buildup ratio	$BR \equiv \frac{Q_d}{Q_b}$	≥ 0
Cohesive/ Critical fracture strength	$\sigma_c = -\frac{\tau_c L}{b\Delta P}$	≥ 0
Distance from end of sample or die	$\varsigma = \frac{y}{L}$	≥ 0

Distance from slip interface	$\zeta = \frac{x}{b}$	$-a \le \zeta \le 1$
Drool layer (cohesive) / wall thickness (adhesive)	$a = \frac{d}{b}$	≥ 0
Drool to bulk thermal conductivity ratio	$K' \equiv \frac{k_d}{k_b}$	≥ 0
Interfacial heat flux	$F = \frac{q_i b}{k T_0}$	≥ 0
Péclet number, ratio of convective to conductive heat transfer, pressure-driven flow	$\text{Pé} \equiv \frac{v_{\max} b^2}{\alpha_f L}$	≥ 0
Péclet number, ratio of convective to conductive heat transfer, simple shear flow	$\text{Pé} \equiv \frac{v_w b^2}{\alpha_f L}$	≥ 0
Ratio of temperature rise from slip heating to temperature rise from slip heating + viscous dissipation	$\Phi \equiv \frac{\Delta T_{SH}}{\Delta T_{SHVD}}$	≥ 0
Ratio of viscous dissipation to slip heating	$\text{Gi} \equiv \frac{\mu h}{2 u_s \tau_c} \left[\frac{\partial v_y}{\partial x} \right]^2$	≥ 0
Shear stress	$\sigma \equiv -\frac{\tau L}{b \Delta P}$	≥ 0
Slip velocity, pressure-driven flow	$\varphi_s \equiv -\frac{v_s \mu_w L}{b^2 \Delta P}$	≥ 0
Slip velocity, simple shear	$\phi_s \equiv \frac{u_s}{v_w}$	$0 \le \phi_s \le 1$
Slit width	$W \equiv \frac{w}{b}$	≥ 0
Time	$\psi = \frac{t\alpha}{b^2}$	≥ 0
Unit normal vector to slip plane	$\vec{n} = \frac{\vec{A}}{\lvert\vec{A}\rvert}$	$\lvert\vec{n}\rvert = 1$
Velocity, bulk	$\varphi_b \equiv -\frac{v_b \mu_w \Delta P}{\tau_c^2 L}$	≥ 0
Velocity, drool	$\varphi_d \equiv -\frac{v_d \mu_w \Delta P}{\tau_c^2 L}$	≥ 0
Velocity, maximum normalized	$\phi \equiv \frac{v}{v_{max}}$	$0 \le \phi \le 1$
Velocity, pressure-driven flow	$\varphi \equiv -\frac{v_f \mu L}{b^2 \Delta P}$	≥ 0

Velocity, simple shear	$\phi \equiv \frac{v_y}{v_w}$	$0 \le \phi \le 1$
Viscosity	$\eta \equiv \frac{\mu}{\mu_w}$	≥ 0
Volumetric flow rate, bulk	$Q_b \equiv -\frac{\dot{V}_b \mu_w L}{b^4 \Delta P}$	≥ 0
Volumetric flow rate, drool	$Q_d \equiv -\frac{\dot{V}_d \mu_w L}{b^4 \Delta P}$	≥ 0
Wall to fluid thermal conductivity ratio	$K \equiv \frac{k_m}{k_f}$	≥ 0

Chapter 1. Introduction

When one body slips on another, heat is generated at the slipping interface. We call this *slip heating* and develop slip heating theory as it applies to cohesive and adhesive slip in extrusion dies. Although we focus on slip in polymer processing, the boundary conditions and theory developed for slip heating apply to any slipping system.

We first consider the relevant slip boundary conditions. For slit flow (see Figure 1), the product of the slip speed, u_s, and the shear stress, τ_{yx}, at the slipping interface is the heat flux, q_x, from the slip boundary (see Table 1 for variable definitions):

$$q_x = u_s \tau_{yx}\Big|_{x=0} \tag{1}$$

which applies to frictional heating at a slipping interface (see Sections 2.9. (i) and 10.7. VI-VII. [2]; see also Example 12., p. 240 of [3]). More generally, the slip speed is the magnitude of the velocity difference between slipping bodies at the slipping interface (e.g. an extruded fluid and the die wall):

$$u_s = \left|\vec{v}_f - \vec{v}_w\right| \tag{2}$$

The work done by the wall on a slipping fluid is given by:

$$\tilde{W} = \vec{F}^T \cdot \vec{d} \tag{3}$$

where $\vec{F}$ is the force exerted by the wall on the fluid, and $\vec{d}$ is the fluid displacement with respect to the wall. So, the power is:

$$\frac{d\tilde{W}}{dt} = \vec{F}^T \cdot \frac{d\vec{d}}{dt} \tag{4}$$

and thus, the corresponding heat liberated by slip at the wall is given by:

$$\dot{Q} = \vec{A}^T \cdot \boldsymbol{\tau}^T \cdot \vec{u}_s \tag{5}$$

so that the resulting heat flux magnitude is:

$$q_i = \vec{n}^T \cdot \boldsymbol{\tau}^T \cdot \vec{u}_s \tag{6}$$

and, the associated heat flux vector for a slipping interface is given by:

$$\vec{q} = q_i \vec{n} = \vec{n} \cdot \vec{n}^T \cdot \boldsymbol{\tau}^T \cdot \vec{u}_s \tag{7}$$

where $\boldsymbol{\tau}$ is the extra stress tensor and $\vec{n}$ is a unit vector normal to the slipping interface (see Section 9-1 of [4]).

We solve the heat transfer problem using the coordinate system outlined in Figure 2. These coordinates are easily rotated into the flow problem presented in Figure 1. Since the heat transfer problem was solved before considering the flow problem, we use non-traditional coordinates where x is transverse to the flow (but in the direction of heat flux) and y is in the die flow direction. In the subsequent chapters, we examine the effect of slip heating in die drool, or cohesive slip, (Chapter 2) and wall slip (Chapter 3), and we provide worked examples showing the use of our slip heating theory in extrusion calculations. Additionally, this work resulted in three publications cited as [5], [6] and [7].

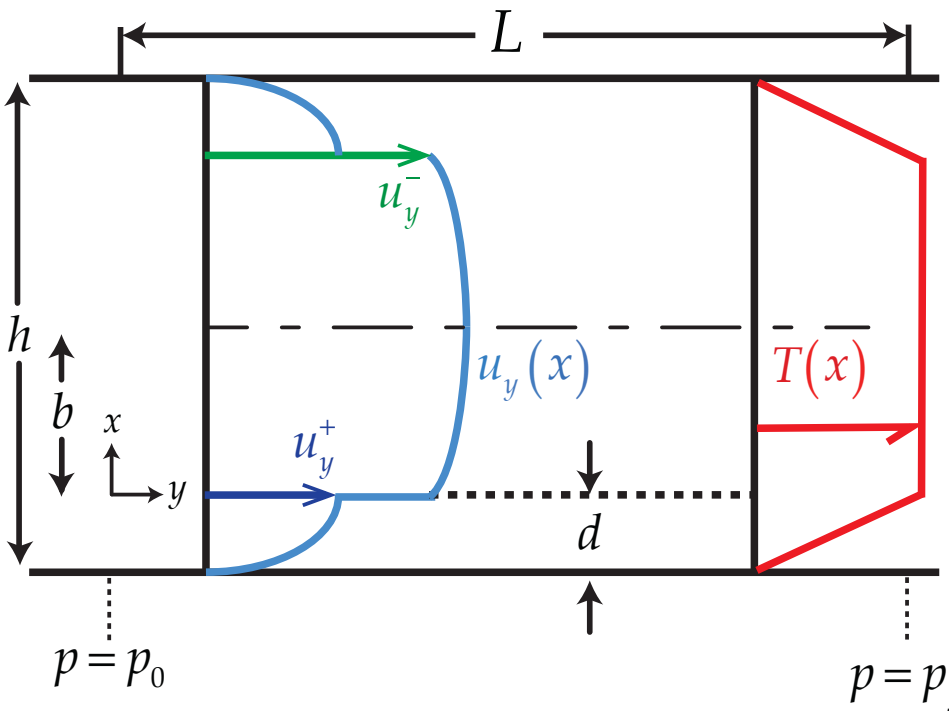

Figure 1: Velocity profiles and concomitant steady temperature profiles. Slip heating between the bulk and the drool layer diminishes drool.

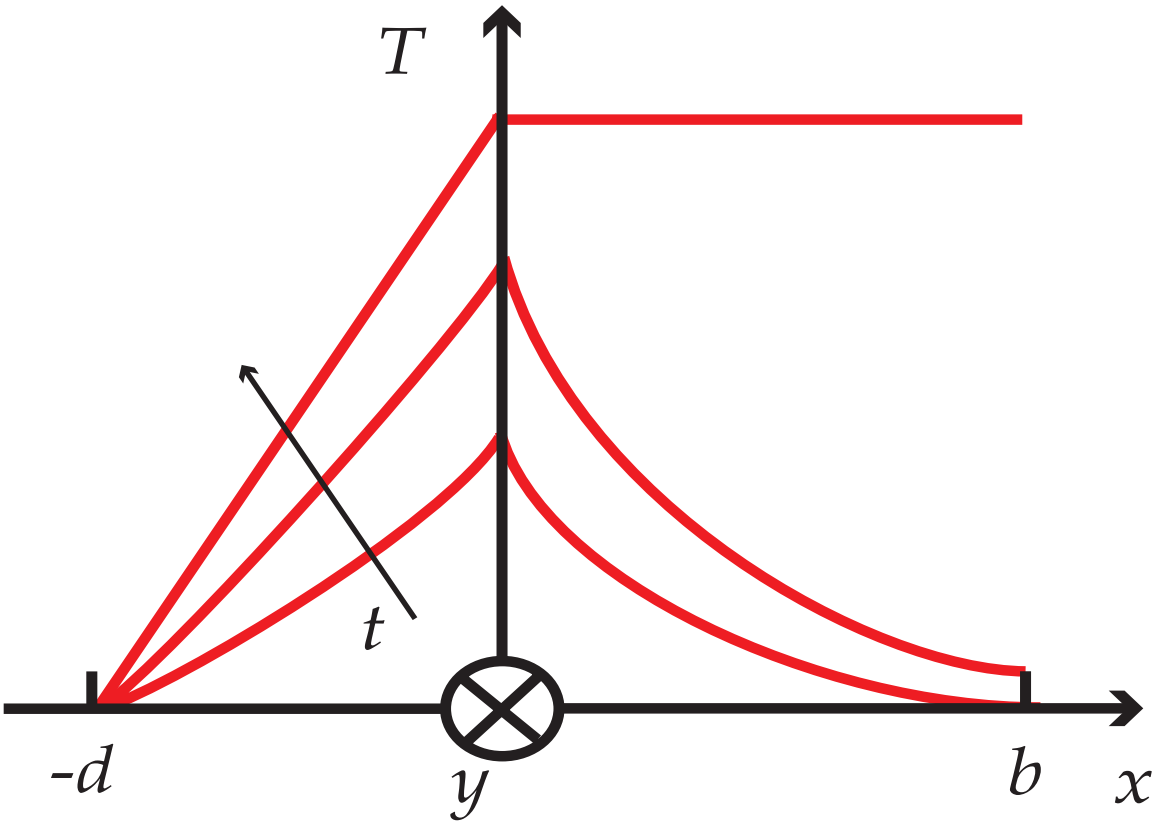

Figure 2: Rotated axis coordinate system, where x as the direction of heat transfer for several temperature profiles in red. The y coordinate (into the page) represents the direction of fluid flow. Compare to Figure 1 showing the flowing system.

Chapter 2. Cohesive Slip Heating

When molten plastic is extruded from a die, it can collect on the open die face (see Figure 3). This accumulation can then interfere with the extrusion, scratching imperfections into the extrudate surfaces called *die lines* [8]. This die face buildup, called *die drool*, costs plastics manufacturers by requiring chemical engineers to shutdown the operation for die cleaning ([9,10,11,12,13]; see Section 8.3.3.3 of [14]). No single governing dimensional parameter has been identified to control die drool, and since changing a system property, such as increasing melt temperature, can result in either an increase or decrease in die drool rate, solving die drool problems is clearly a complex matter (see Result column in TABLE 1. of [15], which we include as Figure 4). This problem can resemble the encrustation of a showerhead with minerals from hard water. For iconic time-lapse videography of die drool, see Video S1 of [16], which we provide images from in Figure 5. Die drool has been attributed to cohesive failure within the fluid at an internal surface where the fluid slips on itself (see Figure 1 and Figure 3); the corresponding *isothermal* analysis of this *drool layer* led to an analytical solution for the drool rate [15]. The fluid within the drool layer creeps along the die wall and accumulates on the die face as drool [15,17]. Cohesive melt failure has also been observed in conjunction with melt fracture (see Figure 6. and EPAPS on-line video for Figure 5 in [18], Figure 5.17 of [19], and section 2.3 of [20]). Additives are often used to suppress die drool and to alleviate other processing problems [21]. These processing aids can intervene at the wall, but may also intervene at the cohesive slip interface. In this paper, we account for the frictional heating at the cohesive slip interface, which we call *slip heating*.

Schmalzer and Giacomin [15,17] allow for the drool composition to differ from that of the bulk, and so do we in Section 2.1.6 below. Both our analysis, and the analysis of Schmalzer and Giacomin [15,17] upon which our analysis relies, are silent on the mass flux at the cohesive slip interface (which may or may not [16] be zero). We further suppose that the entanglement concentration at the cohesive slip interface is zero or nearly so, though this does not enter into our analysis below.

Although cohesive slip can happen with or without wall slip (compare Section 4.5 with 4.4 of [15]; [22]), we do not consider the more complex case where wall slip intervenes. Each fluid has a characteristic cohesive fracture strength that determines not only the cohesive slip velocity, but also the drool layer thickness, and thus the velocity profile within the drool layer [15]. Accurate drool rate prediction can help chemical engineers design dies with minimal down time for cleaning. Specifically, we derive an analytical solution for the developing temperature profiles in the drool layer and in the bulk fluid (see Figure 4), and we then investigate how slip heating affects drool rate.

By applying an Arrhenius model for temperature-dependent viscosity in the drool layer [23,24], an analytical expression for drool rate is obtained that accounts for heating at the slip interface. This analytical solution couples the energy equation and the fluid flow.

We focus on slit flow, which is used for film casting, sheet extrusion, curtain coating, and in many other chemical engineering unit operations. Specifically, we present the solution for heat transfer in pressure-driven slit flow subject to constant heat generation at the cohesive slip interface.

2.1. Slip Heating in Die Drool Without Viscous Dissipation

We solve the energy equation in Cartesian coordinates for both the transient and steady temperature profiles, in both the drool layer and in the bulk polymer. For this simplest relevant non-isothermal problem, we neglect viscous dissipation and convective heating in the melt and we model viscosity as an Arrhenius function of temperature. This temperature dependence of viscosity causes the coupling between the fluid flow and the temperature rise. We conclude by providing three worked examples showing the relevance of slip heating in determining die drool flow rates.

2.1.1. Method

Figure 1 and Table 1 define the Cartesian coordinates for pressure-driven slit flow, where d is the drool layer thickness, and is given by (see Eq. (9) of [15]):

$$d = \frac{h}{2} + \frac{\tau_c L}{\Delta P} \tag{8}$$

which implies the necessary condition for drool:

$$d > 0 \tag{9}$$

which, in turn, implies a minimum gap for drool:

$$h > -\frac{2\tau_c L}{\Delta P} \tag{10}$$

In Eq. (8), we assume d to be constant, which we expect for fully developed flow. Eq. (10) is consistent with nine of the $Q_d(Q)$ entries in TABLE 1. of [15], where increasing Q is found to increase Q_d.

We begin with the y – component of the dimensional equation of motion in terms of the extra stress (Eq. (B.5-2) of [24]):

$$\rho\left(\frac{\partial v_y}{\partial t}+v_x\frac{\partial v_y}{\partial x}+v_y\frac{\partial v_y}{\partial y}+v_z\frac{\partial v_y}{\partial z}\right)=-\frac{\partial p}{\partial y}-\left[\frac{\partial \boldsymbol{\tau}_{xy}}{\partial x}+\frac{\partial \boldsymbol{\tau}_{yy}}{\partial y}+\frac{\partial \boldsymbol{\tau}_{zy}}{\partial z}\right]+\rho g_y \tag{11}$$

which, for $\vec{u}=\left(0,u_y,0\right)$, reduces to:

$$0=-\frac{dp}{dy}-\frac{d\boldsymbol{\tau}_{xy}}{dx} \tag{12}$$

for steady flow. Substituting Newton's law of viscosity:

$$\boldsymbol{\tau}_{xy}=-\mu\frac{dv_y}{dx} \tag{13}$$

into Eq. (12), we obtain the velocity dependent expression:

$$0=-\frac{dp}{dy}+\frac{d}{dx}\left(\mu\left(T\right)\frac{dv_y}{dx}\right) \tag{14}$$

For polymers, when the molecular weight falls below the critical value for entanglement, the fluid behavior is nearly Newtonian. This often applies to commercial grades of condensation polymers such as polyamides, polyesters, and polycarbonates. It may also apply to the drool layer in many higher molecular weight polymeric liquids, since the drool may sometimes result from polymer degradation. Integrating Eq. (14) over y yields:

$$\frac{\Delta p}{L}=\frac{d}{dx}\left(\mu\left(T\right)\frac{dv_y}{dx}\right) \tag{15}$$

Inserting the dimensionless quantities from Table 2 into Eq. (15) produces the dimensionless velocity profile:

$$1=\frac{d}{d\xi}\left(-\eta\left(\Theta\right)\frac{d\varphi}{d\xi}\right) \tag{16}$$

The dimensional equation of energy in terms of heat flux is (Eq. B.8-1 [24]):

$$\rho\hat{C}_p\left(\frac{\partial T}{\partial t}+v_x\frac{\partial T}{\partial x}+v_y\frac{\partial T}{\partial y}+v_z\frac{\partial T}{\partial z}\right)=-\left[\frac{\partial q_x}{\partial x}+\frac{\partial q_y}{\partial y}+\frac{\partial q_z}{\partial z}\right]-\left(\frac{\partial \ln\rho}{\partial \ln T}\right)_p\frac{Dp}{Dt}-\left(\boldsymbol{\tau}:\nabla\mathbf{v}\right) \tag{17}$$

where the viscous heating term reduces to (using Eq. A.7-1 (C) of [24]):

$$-\left(\boldsymbol{\tau}:\nabla\mathbf{v}\right)=-\boldsymbol{\tau}_{yx}\frac{\partial v_y}{\partial x} \tag{18}$$

Inserting Eq. (18) and Fourier's law of heat conduction:

$$q_x=-k\frac{\partial T}{\partial x} \tag{19}$$

into Eq. (17), we obtain:

$$\rho\hat{C}_p\left(\frac{\partial T}{\partial t}+v_x\frac{\partial T}{\partial x}+v_y\frac{\partial T}{\partial y}+v_z\frac{\partial T}{\partial z}\right)=k\left[\frac{\partial^2 T}{\partial x^2}+\frac{\partial^2 T}{\partial y^2}+\frac{\partial^2 T}{\partial z^2}\right]-\left(\frac{\partial \ln\rho}{\partial \ln T}\right)_p\frac{Dp}{Dt}-\boldsymbol{\tau}_{yx}\frac{\partial v_y}{\partial x} \tag{20}$$

Evaluating Eq. (20) for constant ρ and inserting Eq. (13), we find:

$$\rho\hat{C}_p\left(\frac{\partial T}{\partial t}+v_x\frac{\partial T}{\partial x}+v_y\frac{\partial T}{\partial y}+v_z\frac{\partial T}{\partial z}\right)=k\left[\frac{\partial^2 T}{\partial x^2}+\frac{\partial^2 T}{\partial y^2}+\frac{\partial^2 T}{\partial z^2}\right]+\mu\frac{\partial v_y}{\partial x}\frac{\partial v_y}{\partial x} \tag{21}$$

Eq. (21) reduces to:

$$\rho\hat{C}_p\left(\frac{\partial T}{\partial t}+v_y\frac{\partial T}{\partial y}\right)=k\frac{\partial^2 T}{\partial x^2}+\mu\frac{\partial v_y}{\partial x}\frac{\partial v_y}{\partial x} \tag{22}$$

Inserting the dimensionless groups from Table 2 into Eq. (22), we obtain:

$$\frac{\partial\Theta}{\partial\psi}+\phi\frac{v_{\max}b^2}{\alpha L}\frac{\partial\Theta}{\partial\varsigma}=\frac{\partial^2\Theta}{\partial\xi^2}+\mathrm{Br}\frac{\partial\varphi}{\partial\xi}\frac{\partial\varphi}{\partial\xi} \tag{23}$$

where:

$$\mathrm{Br}\equiv\frac{\mu}{kT_0}\left(\frac{b^2\Delta P}{L\mu_w}\right)^2=\frac{\tau_c^4L^2}{kT_0\mu_w\left(\Delta P\right)^2} \tag{24}$$

The convective heating can be neglected when the magnitude of the second term on the left of Eq. (23) is much smaller than either the transient or the conductive

terms. This provides a pair of sufficient conditions for neglecting convective heating in the drool layer:

$$\frac{\partial\Theta_d/\partial\varsigma}{\partial\Theta_d/\partial\psi} \ll \frac{\alpha L}{v_{d,\max} b^2} \tag{25}$$

$$\frac{\partial\Theta_d/\partial\varsigma}{\partial^2\Theta_d/\partial\zeta^2} \ll \frac{\alpha L}{v_{d,\max} b^2} \tag{26}$$

and another pair of sufficient conditions for neglecting convective heating in the bulk layer:

$$\frac{\partial\Theta_b/\partial\varsigma}{\partial\Theta_b/\partial\psi} \ll \frac{\alpha L}{v_{b,\max} b^2} \tag{27}$$

$$\frac{\partial\Theta_b/\partial\varsigma}{\partial^2\Theta_b/\partial\zeta^2} \ll \frac{\alpha L}{v_{b,\max} b^2} \tag{28}$$

When at least one condition in each pairing is met, neglecting convective heating will not introduce inaccuracy in the solutions presented in this paper. In this paper, t is thus the operation time, and t is not to be confused with the melt die residence time.

From Eq. (23) we learn that:

$$\mathrm{Br} \ll 1 \tag{29}$$

is a sufficient condition for accurately neglecting viscous dissipation for the slit flow of Newtonian fluids. For non-Newtonian fluids, Eq. (24) can be reformulated following the method outlined in Table 4.4-1 of [25]. Typically $d \ll b$, so that $b \approx h/2$, which allows Br to be estimated *a priori*.

For slip heating, we arrive at a second sufficient condition by comparing the heat flux from the slipping interface to the viscous heating. This yields the dimensionless group:

$$\mathrm{Gi} \equiv \frac{\mu h}{2u_s \tau_{yx}\Big|_{x=0}}\left[\frac{\partial v_y}{\partial x}\right]^2 = \frac{\mu h}{2u_s \tau_c}\left[\frac{\partial v_y}{\partial x}\right]^2 = -\frac{h^2 \Delta P}{4u_s \tau_c L} \tag{30}$$

where, by definition, the fluid cohesive fracture strength, τ_c, is equal to the shear stress at the slipping interface. Eq. (30) implies that $\mathrm{Gi} \ll 1$ is a second sufficient condition for accurately neglecting viscous dissipation, and thus for the accurate use of our results for Newtonian fluids. For non-Newtonian fluids, Eq. (30) must be reformulated. For pressure-driven capillary flow, an interesting recent study includes adhesive slip and viscous heating, but neglects slip heating (see Eqs. (2)-(6) of [26]).

2.1.2. Transient Temperature Rise

Figure 1 illustrates the velocity profiles in the drool layer and in the bulk fluid, and also, the corresponding temperature profiles that develop when the bulk fluid slips against the drool. The temperature profiles neglecting viscous dissipation are obtained by solving the one-dimensional boundary value problem:

$$\frac{\partial \Theta}{\partial \psi} = \frac{\partial^2 \Theta}{\partial \xi^2} \tag{31}$$

where the exterior wall, $\xi = -a \equiv -d/b$, is isothermal and where there is a heat flux from the slipping interface, $\xi = 0$, given by Eq. (1). The solution is presented for the case where the melt enters and starts at a uniform temperature, T_0, and the wall is maintained at this same temperature, $T_w = T_0$. Using the dimensionless

variables defined in Table 2, the equation of energy (written in terms of temperature) in Cartesian coordinates (see Eq. B.9-1 [24]) reduces to:

$$\frac{\partial \Theta_d(\xi,\psi)}{\partial \psi} = \frac{\partial^2 \Theta_d(\xi,\psi)}{\partial \xi^2}; -a \le \xi \le 0 \tag{32}$$

for the drool layer, and for the bulk fluid:

$$\frac{\partial \Theta_b(\xi,\psi)}{\partial \psi} = \frac{\partial^2 \Theta_b(\xi,\psi)}{\partial \xi^2}; 0 \le \xi \le 1 \tag{33}$$

with the initial condition:

$$\Theta_d(\xi,0) = \Theta_b(\xi,0) = 0 \tag{34}$$

and with the following boundary conditions. For the isothermal wall, we impose:

$$\Theta_d(-a,\psi) = 0 \tag{35}$$

and at the cohesive slip interface, we have both temperature continuity:

$$\Theta_d(0,\psi) = \Theta_b(0,\psi) \tag{36}$$

and the heat flux caused by sliding friction:

$$\left.\frac{\partial \Theta_d}{\partial \xi}\right|_{\xi=0} - \left.\frac{\partial \Theta_b}{\partial \xi}\right|_{\xi=0} = F \tag{37}$$

and finally, the adiabatic mid-plane:

$$\left.\frac{\partial \Theta_b}{\partial \xi}\right|_{\xi=1} = 0 \tag{38}$$

Carslaw solved the special case of two solids where $d = b$ (see Example 12., p. 240 of [3]), but for die drool $d \ll b$. The Laplace transform of Eq. (32) yields:

$$s\bar{\Theta}_d(\xi,s) = \frac{\partial^2 \bar{\Theta}_d(\xi,s)}{\partial \xi^2} \tag{39}$$

Solving Eq. (39) for $\bar{\Theta}_d(\xi,s)$, we find:

$$\bar{\Theta}_d(\zeta,s)=\frac{F}{2s^{3/2}}\left[\frac{\sinh\sqrt{s}\left(1+a+\zeta\right)+\sinh\sqrt{s}\left(a-1+\zeta\right)}{\cosh\sqrt{s}\left(1+a\right)}\right] \tag{40}$$

which is the solution in the Laplace domain. Eq. (40) is then inverted to find the time domain solution (see Appendix I for a detailed derivation of Eqs. (41) and (43)):

$$\Theta_d(\zeta,\psi)=\frac{F}{1+a}\sum_{n=0}^{\infty}\frac{(-1)^n}{\lambda^2}\left[\sin\lambda\left(1+a+\zeta\right)+\sin\lambda\left(a-1+\zeta\right)\right]\left(1-e^{-\lambda^2\psi}\right);-a\le\zeta\le 0 \tag{41}$$

where:

$$\lambda\equiv\frac{2n+1}{2\left(1+a\right)}\pi \tag{42}$$

This solution applies in the drool layer, between the die wall, $\zeta=-a$, and the slipping interface, $\zeta=0$. Figure 7 illustrates the drool layer temperature profile predicted by Eq. (41). Solving for the bulk fluid temperature profile by the same method, we obtain:

$$\Theta_b(\zeta,\psi)=\frac{F}{1+a}\sum_{n=0}^{\infty}\frac{(-1)^n}{\lambda^2}\left[\sin\lambda\left(1+a-\zeta\right)+\sin\lambda\left(a-1+\zeta\right)\right]\left(1-e^{-\lambda^2\psi}\right);0\le\zeta\le 1 \tag{43}$$

This solution for the bulk fluid applies between the slip interface and the fluid mid-plane, $0\le\zeta\le 1$, and Figure 8 shows this temperature profile. In their limits as $b,d\to\infty$, Eqs. (41) and (43) match the solution forms of Yevtushenko and Kuciej [27] for frictional heating between semi-infinite solid blocks, as they should.

By setting $\zeta=0$ in either temperature profile, we obtain the time dependent expression for the interface temperature, which is presented in Figure 9 for different values of dimensionless time, ψ:

$$\Theta_i \equiv \Theta_d(0,\psi) = \frac{F}{1+a}\sum_{n=0}^{\infty}\frac{(-1)^n}{\lambda^2}\left[\sin\lambda(1+a)+\sin\lambda(a-1)\right]\left(1-e^{-\lambda^2\psi}\right) \tag{44}$$

As expected, a steady state is reached soon after $\psi = 1$. The sigmoidal shape of this curve indicates a period of rapid heating until $\psi \approx 0.1$, which signals the transition from a linear interfacial heating period to an exponential decaying temperature rise.

Since Θ_i corresponds to the hottest point in the flow field, practitioners will seek to at least keep Θ_i below the dimensionless melt degradation point:

$$\Theta_D \equiv \frac{T_D - T_0}{T_0} \tag{45}$$

In other words, we do not want to degrade the material near the extrudate surface. Because the drool layer interface is the hottest point in the flow field, collected die drool is normally severely degraded polymer. Eq. (44) is thus a main result of this work.

2.1.3. Steady Temperature Rise

If the limits are taken of Eqs. (41) and (43) as $\psi \to \infty$, we obtain:

$$\Theta_{d,\infty}(\xi) = F(\xi + a);\ -a \le \xi \le 0 \tag{46}$$

$$\Theta_{b,\infty}(\xi) = Fa;\ 0 \le \xi \le 1 \tag{47}$$

which are the steady state drool layer and bulk fluid temperature profiles. More general steady state profiles can be acquired for the case of an isothermal wall of arbitrary temperature, Θ_w:

$$\Theta_{d,\infty}(\xi) = F(\xi + a) + \Theta_w;\ -a \le \xi \le 0 \tag{48}$$

$$\Theta_{b,\infty}(\xi) = Fa + \Theta_w;\ 0 \le \xi \le 1 \tag{49}$$

but, for the transient case, this lies beyond the scope of this work. At steady state, the heat generated at the interface is removed entirely by the isothermal wall. This in turn prevents thermal runaway, since the bulk fluid temperature is maintained at the interface temperature.

2.1.4. Die Drool Flow Rate

Since the predicted temperature rise lowers the drool viscosity, the temperature rise affects the drool rate. The steady state drool layer velocity profile for pressure-driven flow through a slit is found by solving the equation of motion for a temperature dependent viscosity following a method outlined in Example 11.4-3 of [24]. Using the dimensionless variables defined in Table 2, the equation of motion (written in terms of velocity) in Cartesian coordinates (see Eq. B.6-2 [24]) reduces to:

$$1 = \frac{d}{d\xi}\left(-\eta\left(\Theta_d\right)\frac{d\varphi}{d\xi}\right) \tag{50}$$

where the temperature-dependence of the viscosity is given by:

$$\eta(T) \equiv \frac{\mu(T)}{\mu_w} = \exp\left[B\left(\frac{1}{T} - \frac{1}{T_w}\right)\right] \cong \exp\left[-B\left(\frac{T - T_w}{T_{i,\infty}T_w}\right)\right] \tag{51}$$

where B is its temperature-sensitivity, and where T_w is the wall temperature. The approximation in Eq. (51) is reasonable for small differences between T_w and the slipping interface temperature, $T_{i,\infty}$ [24]. By inserting the dimensionless quantities from Table 2 and solving for the viscosity at the interface, we obtain:

$$\eta_{i,\infty} = \exp\left[-\beta\left(\frac{\Theta_{i,\infty} - \Theta_w}{\Theta_w + 1}\right)\right];\ \beta \equiv B / T_{i,\infty} \tag{52}$$

Combining Eq. (51) and Eq. (52), we find:

$$\eta\left(\Theta_d\right) = \eta_{i,\infty}^{\frac{\Theta_d - \Theta_w}{\Theta_{i,\infty} - \Theta_w}} = \eta_{i,\infty}^{1+\zeta/a} \tag{53}$$

Inserting Eq. (53) into Eq. (50) and solving subject to the boundary conditions:

$$\left.\frac{d\varphi}{d\zeta}\right|_{\zeta=0} = \frac{\sigma_c}{\eta_{i,\infty}} \tag{54}$$

for the slipping interface, and:

$$\varphi\left(-a\right) = 0 \tag{55}$$

for the wall, we obtain the steady state drool layer velocity profile (see Figure 10):

$$\varphi_d\left(\zeta\right) = \frac{a}{\left(\ln\eta_{i,\infty}\right)^2}\left[\eta_{i,\infty}^{-(1+\zeta/a)}a + \eta_{i,\infty}^{-(1+\zeta/a)}\ln\eta_{i,\infty}\left(\zeta - \sigma_c\right) - a + \ln\eta_{i,\infty}\left(\sigma_c + a\right)\right];\ -a \le \zeta \le 0 \tag{56}$$

In Eq. (54), σ_c is the dimensionless cohesive fracture strength defined in Table 2. Interestingly, σ_c is always unity regardless of the values of τ_c, ΔP, and L. This is a result of the countering effect of b, which changes proportionally with τ_c, ΔP, and L to always maintain $\sigma_c = 1$.

Integrating Eq. (56) over the drool layer cross section gives the dimensionless volumetric drool flow rate:

$$Q_d = \frac{a^2 W}{\eta_{i,\infty}\left(\ln\eta_{i,\infty}\right)^2}\left[\eta_{i,\infty}\left(a + \sigma_c\right)\ln\eta_{i,\infty} - 2a\eta_{i,\infty} + \left(1 - \eta_{i,\infty}\right)\sigma_c + \frac{2a\left(\eta_{i,\infty} - 1\right)}{\ln\eta_{i,\infty}}\right];\ -a \le \zeta \le 0 \tag{57}$$

Similarly, we obtain the bulk melt velocity profile shown in Figure 11:

$$\varphi_b\left(\zeta\right) = -\frac{1}{2\eta_b}\zeta^2 + \frac{1}{\eta_b}\zeta + \frac{a}{\left(\ln\eta_{i,\infty}\right)^2}\left[\frac{a - \sigma_c\ln\eta_{i,\infty}}{\eta_{i,\infty}} - a + \ln\eta_{i,\infty}\left(\sigma_c + a\right)\right] + \varphi_s;\ 0 \le \zeta \le 1 \tag{58}$$

and the corresponding bulk melt volumetric flow rate is:

$$Q_b = W\left(\frac{1}{3\eta_b} + \frac{a}{\left(\ln\eta_{i,\infty}\right)^2}\left[\frac{a+\sigma_c\ln\eta_{i,\infty}}{\eta_{i,\infty}} - a + \ln\eta_{i,\infty}\left(\sigma_c + a\right)\right] + \varphi_s\right); 0 \le \zeta \le 1 \tag{59}$$

Following Gander [28], we normalize the drool flow rate with bulk flow rate to obtain the *buildup ratio*:

$$BR \equiv \frac{Q_d}{Q_b} \tag{60}$$

which the plastics engineer will use, and is thus a main result of this paper.

Figure 12 shows the dependence of buildup ratio, BR, on cohesive fracture strength, τ_c, and thermal sensitivity, β. As τ_c decreases, BR increases rapidly because the fluid fractures more easily into drool and bulk layers. Increasing thermal sensitivity delays the effect of decreasing τ_c by making viscosity more temperature-dependent, which creates a greater difference in bulk and drool layer viscosities. Remarkably, in temperature-sensitive systems (where $\beta > 35$), the buildup ratio is not monotonic with the cohesive strength. This result of our slip heating theory would appear to explain why buildup problems are sometimes difficult to troubleshoot (see Result column in TABLE 1 of [15]). When $\beta \le 1$, melt thermal sensitivities do not affect BR, and thus, $\beta = 1$ is a reasonable choice for many melts and is used in the following worked examples.

2.1.5. Worked Example 1: Sheet extrusion drool rate without degradation

A plastic sheet manufacturer aims to estimate the steady drool rate for a new material to be considered for her extrusion operation. For this, she knows that

$T_0 = T_w = 423\ \text{K}$, $h = 6\ \text{mm}$, $\tau_c = 0.18\ \text{MPa}$, $u_s = 300\,\text{mm/s}$, $k = 0.1\ \text{W/m-K}$, $\tilde{C}_p = 2.0\ \text{J/g-K}$, $\rho = 0.90\ \text{g/mL}$, $\mu_w = 600\ \text{Pa-s}$, $L = 50\ \text{mm}$, $\Delta P = -31\ \text{MPa}$, and $w = 1.0\ \text{m}$, which are reasonable values for a PP sheet extrusion process (see **Table 25-18** [29]). She assumes that the drool is hardly degraded and thus has it to have the same rheology as the bulk melt.

Using Eq. (30), she first calculates $\text{Gi} = 0.320$, and Eq. (24), $\text{Br} = 0.106$, which satisfies the sufficient condition given by Eq. (29). She then determines the drool layer thickness using Eq. (18) of [15]:

$$d = \frac{h}{2} + \frac{\tau_c L}{\Delta P} = 9.7\ \mu\text{m} \tag{61}$$

Thus, the bulk fluid thickness is:

$$b = \frac{h}{2} - d = 0.29\ \text{mm} \tag{62}$$

Applying these values and the values provided, she calculates the heat generation at the interface:

$$q_i = u_s \tau_c = 54.0\ \text{kW/m}^2 \tag{63}$$

and then its dimensionless value:

$$F = \frac{q_i b}{k T_0} = 0.371 \tag{64}$$

and the dimensionless drool thickness:

$$a = \frac{d}{b} = 0.033 \tag{65}$$

The dimensionless temperature profiles for the drool and bulk layers become:

$$\Theta_{d,\infty}(\xi) = 0.371\left(\xi + 0.033\right);\ -a \le \xi \le 0 \tag{66}$$

$$\Theta_{b,\infty}(\zeta) = \Theta_{i,\infty} = 1.24 \times 10^{-2};\ 0 \le \zeta \le 1 \tag{67}$$

The latter corresponds to a $\Delta T = 5.23\,\mathrm{K}$. Inserting Eq. (67) into Eq. (52) $\eta_{i,\infty}$ and setting $\beta = 1$, she finds:

$$\eta_{i,\infty} = \eta_b = \exp\left(-\Theta_{i,\infty}\right) = 0.988 \tag{68}$$

Additionally, she finds the dimensionless fracture strength and slip velocity to be:

$$\sigma_c = -\frac{\tau_c L}{b\Delta P} = 1 \tag{69}$$

$$\varphi_s = -\frac{v_s \mu_w \Delta P}{\tau_c^2 L} = 3.44 \tag{70}$$

Substituting Eqs. (69), (68) and (65) into Eq. (57), she obtains the dimensionless volumetric drool flow rate:

$$Q_d = 1.96;\ -a \le \zeta \le 0 \tag{71}$$

Similarly, inserting Eqs. (69), (68) and (65) into Eq. (59) yields the dimensionless volumetric bulk flow rate:

$$Q_b = 1.31 \times 10^4;\ 0 \le \zeta \le 1 \tag{72}$$

Taking the ratio of Eq. (71) and Eq. (72), she finally obtains the buildup ratio:

$$BR = \frac{Q_d}{Q_b} = 1.49 \times 10^{-4} \tag{73}$$

Lastly, she finds the time it takes to reach the steady buildup ratio:

$$t = \frac{\psi b^2}{\alpha} \gg 1.52\,\mathrm{s} \tag{74}$$

and thus, she expects the buildup ratio of Eq. (73) to be obtained in about 1 minute. The goal of a plastics engineer is to reduce the buildup ratio to some

critical value governed by the shutdown interval. This critical value is typically between 10^{-6} (for shorter extrusion runs) and 10^{-9} (for the longest runs). The buildup ratio can be decreased by increasing the die length, decreasing the applied pressure gradient (and thus the throughput), or if possible, by thinning the gap.

2.1.6. Worked Example 2: Sheet extrusion drool rate with drool degradation

The same plastics engineer wants to explore the influence of polymer degradation on the drool rate of Example 1. From experience, she expects the degraded drool viscosity to be about 83% of the bulk polymer viscosity. Using the quantities provided in Example 1, including all of the given information, and also the quantities calculated in Eqs. (61) through (67) along with (69) and (70), she calculates the steady buildup ratio for the sheet extrusion (Eq. (74) applies equally to Example 2). Applying the 17% viscosity reduction specifically to Eqs. (57) and (59), she obtains the volumetric drool and bulk flow rates:

$$Q_d = 2.08; -a \le \xi \le 0 \tag{75}$$

$$Q_b = 1.32 \times 10^4; 0 \le \xi \le 1 \tag{76}$$

Using Eqs. (75) and (76) yields:

$$BR = \frac{Q_d}{Q_b} = 1.58 \times 10^{-4} \tag{77}$$

Hence, the drool rate increases when the drool is degraded, because the drool viscosity decreases. It is thus important for plastics engineers to avoid temperatures at the slip interface that could damage the polymer.

2.1.7. Worked Example 3: Sheet extrusion buildup ratio evolution without drool degradation

Another plastics engineer wants to determine the dependence of drool rate on the operation time for the system from Example 1. To ease calculation, he uses a pseudo-steady state approximation, $\Theta_\infty = \Theta(\psi)$, in which he inserts a temperature-dependent viscosity using Eqs. (41) and (43) into the steady velocity profiles (Eqs. (56) and(58)). Figure 13 is the result of his work.

From inspection of Eq. (56), he spots a singularity arising at $\psi = 0$ because $\eta_i(\psi = 0) = 1$. Since BR is negative when $\psi < 10^{-4}$, the pseudo-steady state approximation is invalid at short times. Therefore, Figure 13 can only be used when ψ is not $\ll 1$, which is a sufficient condition for accurate use of his results. As time progresses, the drool layer temperature increases faster than the bulk fluid temperature, and thus, the drool flow rate increases more rapidly than the bulk flow rate. A maximum is reached when the drool layer nearly reaches steady state. For this case, the maximum occurs at $\psi = 1.44 \times 10^{-3}$, and after this point, continued bulk layer heating causes its viscosity to decrease to a steady state value at $\psi \gg 1$. Since $BR = BR(a, \varphi_s, \beta, F, \psi)$, this buildup ratio curve is not universal and only applies to a specific set of physical parameters outlined in Example 1, for which $BR(a, \varphi_s, \beta, F, \psi) = BR(0.0333, 0.0344, 1.00, 0.371, \psi)$. Though this solution is particular to this example, the qualitative behavior of BR with ψ is thought to be similar regardless of system properties.

2.2. Slip Heating in Die Drool With Viscous Dissipation

In Section 2.1, we develop the transient and steady temperature profiles in die drool and analyze their effect on the build-up ratio without accounting for viscous dissipation. Here, we revisit our steady temperature analysis, but for when viscous dissipation matters. We also present a worked example investigating the role of slip heating and viscous dissipation in die drool.

2.2.1. Steady Velocity Profiles in Drool and Bulk Layers

The y – component of the equation of motion in terms of shear stress for Cartesian coordinates (Eq. (B.5-2) of [24]) reduces to:

$$\frac{dp}{dy} = -\frac{d\tau_{xy}}{dx} \tag{78}$$

for pressure-driven flow between closely spaced parallel plates (see Figure 14). For a Newtonian melt with temperature independent viscosity, Eq. (78) becomes:

$$\frac{dp}{dy} = \mu \frac{d^2 v_y}{dx^2} \tag{79}$$

When Eq. (79) is integrated over the length of the die, L, we obtain:

$$\frac{d^2 v_y}{dx^2} = \frac{\Delta p}{L\mu} \tag{80}$$

Substituting the dimensionless groups:

$$\varphi \equiv \frac{-v_y \mu L}{\Delta p b^2} \tag{81}$$

and:

$$\zeta \equiv \frac{x}{b} \tag{82}$$

into Eq. (80) yields:

$$\frac{d^2\varphi}{d\zeta^2} = -1 \tag{83}$$

which applies for both the bulk and drool layers.

For the drool layer velocity, Eq. (83) is subject to the no slip boundary condition at the wall:

$$\varphi_d\left(-d/b\right) \equiv \varphi_d\left(-a\right) = 0 \tag{84}$$

and to the slipping interface condition:

$$\left.\frac{d\varphi_d}{d\zeta}\right|_{\zeta=0} = \sigma_c \equiv \frac{-\tau_c L}{b\Delta p} \tag{85}$$

We find the drool velocity profile:

$$\varphi_d\left(\zeta\right) = \frac{a^2-\zeta^2}{2} + \sigma_c\left(\zeta + a\right) \tag{86}$$

Using the other boundary condition at the slipping interface:

$$\varphi_b\left(0\right) = \varphi_d\left(0\right) + \varphi_s = \frac{a^2}{2} + \sigma_c a + \varphi_s \tag{87}$$

and the mid-plane condition:

$$\left.\frac{d\varphi_b}{d\zeta}\right|_{\zeta=1} = 0 \tag{88}$$

we find the bulk layer velocity profile:

$$\varphi_b\left(\zeta\right) = \frac{a^2-\zeta^2}{2} + \zeta + \sigma_c a + \varphi_s \tag{89}$$

that will be used in Eq. (100) to determine the impact of viscous dissipation on the melt temperature rise.

2.2.2. Results: Steady Temperature Rise from Viscous Dissipation and Slip Heating

The dimensional equation of energy in terms of heat flux in Cartesian coordinates (see Eq. B.8-1 [24]) reduces to:

$$\rho\hat{C}_p v_y \frac{\partial T}{\partial y} = -\frac{\partial q_x}{\partial x} - \left(\boldsymbol{\tau} : \nabla v\right) \tag{90}$$

for time-steady temperature rise where conductive heating in the flow direction is negligible. Using Eq. A.7-1 (C) of [24] to replace $\left(\boldsymbol{\tau} : \nabla v\right)$ in Eq. (90) yields:

$$\rho\hat{C}_p v_y \frac{\partial T}{\partial y} = -\frac{\partial q_x}{\partial x} - \boldsymbol{\tau}_{yx} \frac{\partial v_y}{\partial x} \tag{91}$$

and for a Newtonian fluid, Eq. (91) becomes:

$$\rho\hat{C}_p v_y \frac{\partial T}{\partial y} = k\frac{\partial^2 T}{\partial x^2} + \mu\left(\frac{\partial v_y}{\partial x}\right)^2 \tag{92}$$

Eq. (92) can be rewritten in dimensionless form:

$$-\text{Pé}\varphi \frac{\partial \Theta}{\partial \varsigma} = \frac{\partial^2 \Theta}{\partial \xi^2} + \text{Br}\left(\frac{\partial \varphi}{\partial \xi}\right)^2 \tag{93}$$

where:

$$\Theta \equiv \frac{T - T_0}{T_0} \tag{94}$$

$$\varsigma \equiv \frac{y}{L} \tag{95}$$

$$\text{Br} \equiv \frac{b^4}{\mu k T_0}\left(\frac{\Delta p}{L}\right)^2 \tag{96}$$

and:

$$\text{Pé} \equiv \frac{b^4 \Delta p}{\alpha L^2 \mu} \tag{97}$$

Convective heating can be neglected when:

$$\text{Pé} \ll 1 \tag{98}$$

which is a sufficient condition for the accurate use of our results. A second sufficient condition is satisfied when the temperature gradient along the die falls well below the second derivative of the temperature through the melt:

$$\frac{\partial \Theta}{\partial \varsigma} \ll \frac{\partial^2 \Theta}{\partial \xi^2} \tag{99}$$

When convective heating is small, Eq. (93) reduces to:

$$\frac{d^2 \Theta}{d\xi^2} = -\text{Br}\left(\frac{\partial \varphi}{\partial \xi}\right)^2 \tag{100}$$

which is used below to develop the temperature profiles for the drool and bulk layers.

We solve for the drool and bulk temperature profiles subject to an isothermal die wall:

$$\Theta_d(-a) = \Theta_w \tag{101}$$

an adiabatic mid-plane:

$$\left.\frac{d\Theta_b}{d\xi}\right|_{\xi=1} = 0 \tag{102}$$

temperature continuity at the slipping interface:

$$\Theta_d(0) = \Theta_b(0) \tag{103}$$

and constant heat generation at the slipping interface:

$$K' \left.\frac{d\Theta_d}{d\xi}\right|_{\xi=0} - \left.\frac{d\Theta_b}{d\xi}\right|_{\xi=0} = F \tag{104}$$

where the dimensionless interfacial heat flux is:

$$F \equiv \frac{q_i b}{k_b T_0} \tag{105}$$

and the thermal conductivity ratio is:

$$K' \equiv \frac{k_d}{k_b} \tag{106}$$

The latter allows for different thermal properties of the drool and bulk layers, as in the case of thermal degradation. When there is no degradation or the thermal properties of the drool and bulk layers do not differ, $K = 1$. By integrating Eq. (100) and then applying the above boundary conditions, we find the drool temperature profile:

$$\Theta_d(\xi) = \mathrm{Br}\left(\frac{a^4 - \xi^4}{12} + \sigma_c \frac{\xi^3 - a^3}{3} + \sigma_c^2 \frac{a^2 - \xi^2}{2}\right) + \left(\frac{F}{K'} + \frac{\mathrm{Br}}{3K'}\right)(\xi - a) + \Theta_w \tag{107}$$

and the bulk temperature profile:

$$\Theta_b(\xi) = \mathrm{Br}\left(\frac{a^4 - \xi^4}{12} + \frac{\sigma_c a^3 + \xi^3 + \xi}{3} + \frac{\sigma_c^2 a^2 - \xi^2}{2}\right) + \left(\frac{F}{K'} + \frac{\mathrm{Br}}{3K'}\right)a + \Theta_w \tag{108}$$

These can be used to determine the true temperature of the polymer melt in systems with cohesive slip. Because σ_c is always unity (see section V of [5,30]), we get:

$$\Theta_d(\xi) = \mathrm{Br}\left(\frac{a^4 - \xi^4}{12} + \frac{a^3 + \xi^3}{3} + \frac{a^2 - \xi^2}{2}\right) + \left(\frac{F}{K'} + \frac{\mathrm{Br}}{3K'}\right)(\xi + a) + \Theta_w \tag{109}$$

and:

$$\Theta_b(\xi) = \mathrm{Br}\left(\frac{a^4 - \xi^4}{12} + \frac{a^3 + \xi^3 + \xi}{3} + \frac{a^2 - \xi^2}{2}\right) + \left(\frac{F}{K'} + \frac{\mathrm{Br}}{3K'}\right)a + \Theta_w \tag{110}$$

The maximum melt temperature occurs at the mid-plane, $\xi = 1$:

$$\Theta_{max} \equiv \Theta_b(1) = \mathrm{Br}\left(\frac{a^4+1}{12}+\frac{a^3}{3}+\frac{a^2}{2}\right)+\left(\frac{F}{K'}+\frac{\mathrm{Br}}{3K'}\right)a+\Theta_w \tag{111}$$

It is the goal of the plastics engineer to prevent the maximum temperature rise from exceeding the polymer degradation point. Eq. (110) is a main result of this work, and the following worked example demonstrates its usefulness.

2.2.3. Worked Example: Roles of Slip Heating and Viscous Dissipation in Die Drool

A plastics engineer must determine the role of temperature rise in die drool of her sheet extrusion die. Her system specifications are: $T_0 = T_w = 423\ \mathrm{K}$, $h = 0.3\ \mathrm{mm}$, $\dot{V}_b = 209\ \mathrm{L/h}$, $k_d = k_b = 0.1\ \mathrm{W/m\text{-}K}$, $\tilde{C}_p = 1.6\ \mathrm{J/g\text{-}K}$, $\rho = 0.90\ \mathrm{g/mL}$, $\mu = 600\ \mathrm{Pa\text{-}s}$, $L = 40\ \mathrm{mm}$, $\Delta P = -35\ \mathrm{MPa}$, $w = 1.0\ \mathrm{m}$, and $\tau_c = 0.12\ \mathrm{MPa}$, which are reasonable values for a PP sheet extrusion process (see **Table 25-18** [29]). She has determined the latter value of τ_c from previous die drool measurements (following Sections 8 and 9 of [15]).

She first determines the drool layer thickness (see Eq. 18 of [15]):

$$d \equiv \frac{h}{2}+\frac{\tau_c L}{\Delta p} = 12.9\ \mu\mathrm{m} \tag{112}$$

which corresponds to a bulk layer thickness:

$$b \equiv \frac{h}{2} - d = 0.137\ \mathrm{mm} \tag{113}$$

Integrating Eq. (89) over the bulk layer cross-section, she finds the slip speed to be:

$$u_s = \frac{\dot{V}_b}{2bw} + \frac{\Delta p}{\mu L}\left(\frac{b^2}{3} + db + \frac{d^2}{2}\right) = 200 \text{ mm/s} \tag{114}$$

She calculates the heat generation at the interface from slip heating to be:

$$q_i = u_s \tau_c = 24.0 \text{ kW/m}^2 \tag{115}$$

and then its dimensionless value:

$$F \equiv \frac{q_i b}{k T_0} = 7.78 \times 10^{-2} \tag{116}$$

and the dimensionless drool thickness:

$$a \equiv \frac{d}{b} = 9.38 \times 10^{-2} \tag{117}$$

She then determines the maximum melt temperature in the presence of both slip heating and viscous dissipation, using Eq. (111), to be:

$$\Theta_{\max} = 8.56 \times 10^{-3} \tag{118}$$

which corresponds to a temperature rise from both slip heating (SH) and viscous dissipation (VD) of:

$$\Delta T_{SHVD} = 3.62 \text{ K} \tag{119}$$

By setting $\text{Br} = 0$ in Eq. (111), she obtains an expression for temperature rise from slip heating alone:

$$\Theta_{\max} = aF \tag{120}$$

which matches Eq. (44) of [5]. Using Eq. (120) she gets:

$$\Theta_{\max} = aF = 7.29 \times 10^{-3} \tag{121}$$

which corresponds to a temperature rise of:

$$\Delta T_{SH} = 3.09 \text{ K} \tag{122}$$

Using Eqs. (122) and (119), she next constructs the ratio:

$$\frac{\Delta T_{SH}}{\Delta T_{SHVD}} = 0.851 \tag{123}$$

from which she learns that slip heating is the primary contribution to overall heating.

Because her system may require adjustment, she decides to investigate the relative role of slip heating and viscous dissipation for other system specifications. She thus sets $\Theta_w = 0$ and divides Eq. (111) by the expression in Eq. (120) to develop the ratio of temperature rise from slip heating to the temperature rise from both slip heating and viscous dissipation:

$$\Phi \equiv \frac{\Delta T_{SH}}{\Delta T_{SHVD}} = \left(\frac{\Delta p}{\mu u_s \Xi L} \left(\frac{h^3}{96} - \frac{h^2}{48}\Xi + \frac{h}{24}\Xi^2 + \frac{\Xi^3}{4} + \frac{\Xi^4}{6h + 12\Xi} - \frac{\Xi^3}{3K} \right) + \frac{1}{K'} \right)^{-1} \tag{124}$$

where:

$$\Xi \equiv \frac{\tau_c L}{\Delta p} \tag{125}$$

is a characteristic length. Eq. (124) is a main result of this work. Using Eq. (124) with $K = 1$ she generates Figure 15 showing the fraction of total heating from slip heating as a function of slit width for different die pressure drops. Asymptotes arise at small gaps where the drool layer disappears and slip heating no longer occurs. When the drool layer exists, small die gaps, $h \le 0.1$ mm, have negligible amounts of viscous heating, and as the gap increases viscous heating becomes the primary heating source. The plastics engineer should consider both slip heating and viscous dissipation in thermal analyses of drooling dies except for

very large die gaps, $h \geq 5$ mm, where slip heating can be neglected, and very small die gaps, $h \leq 0.1$ mm, where viscous dissipation can be neglected.

She notes that increasing viscosity or slip speed amplifies the contribution of slip heating to total melt heating. Increasing die length or polymer cohesive fracture strength increases the importance of viscous dissipation for small gaps but expands the region of slip heating dominance to larger gaps. In other words, increasing these parameters shifts the curves in Figure 15 down and right. As die pressure drop increases, slip heating matters more at low gaps but the threshold where viscous dissipation becomes the major contributor is reduced to smaller gaps.

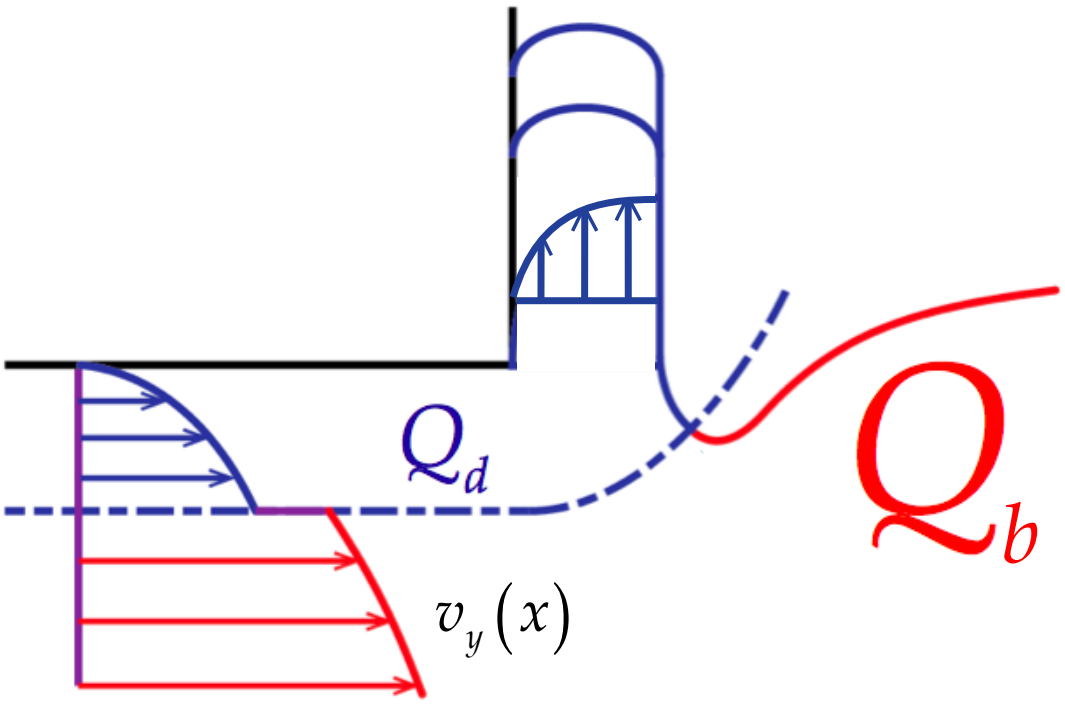

Figure 3: Die drool formed within the die, in a drool layer, flowing onto the die lip. Bulk fluid slips against the drool layer, without wall slip.

Table 1 Literature on die drool rate measurements.

	Extrudate	Material	Experiment	Result	References
Chan (1995)	◎	15% Viton 85% Hytrel	$Q_d(\sigma)$	↑	[16]
Gander (1996), Ding et al. (2000)	bf	LLDPE	BR(PI)	↑	[17, 18]
Gander (1996), Ding et al. (2000)	bf	LLDPE	BR(φ)	↑↓	[18]
Chai (2001)	⊙	LLDPE	$Q_d(Q)$	↑↓	[19]
Chai (2001)	⊙	LLDPE	$Q_d(C_{LDPE})$	↓	[19]
Chaloupková and Zatloukal (2006, 2007), Chaloupková (2007)	⊙	mLLDPE	$Q_d(Q)$	↑↓	[20–22]
Chaloupková and Zatloukal (2007), Chaloupková (2007)	⊙	mLLDPE	$Q_d(T)$	↓↑	[21, 22]
Hogan et al. (2008)	⊙	MBPE	$Q_d(Q)$	↑	[23]
Hogan et al. (2008)	⊙	MBPE	$Q_d(T)$	↓↑	[23]
Hogan et al. (2008)	⊙	MBPE	$Q_d(L/b)\|_{b,Q}$	↑	[23]
Zatloukal et al. (2008)	⊙	mLLDPE	$Q_d(Q)$	↑↓	[24]
Chaloupková and Zatloukal (2009)	⊙	mLLDPE	$Q_d(Q)$	↑↓	[25]
Musil and Zatloukal (2010, 2011, 2012), Zatloukal and Musil (2011)	⊙	HDPE	$Q_d(Q)$	↑	[9, 10, 12]
Musil et al. (2011)	⊙	HDPE	$Q_d(Q)$	↑	[11]
Zatloukal and Musil (2011)	⊙	HDPE	$Q_d(Q)$	↑	[26]
This paper	//, ◎ and ⊙	All materials	$Q_d(L/b)$ $Q_d(Q)$	↓	

$Y(X)|_Z$, measure variable Y versus controlled variable X holding Z constant; ↑, measured variable increases with controlled variable; ↓, measured variable decreases with controlled variable; ↑↓, measured variable increases, then decreases with controlled variable; ↓↑, measured variable decreases, then increases with controlled variable; //, sheet; ⊙, rod, strand, or fiber; ◎, pipe or tubing; bf, blown film; σ, surface energy of die wall in air; C_{LDPE}, concentration of MFR 2 autoclave LDPE in LLDPE; MBPE, metallocene based polyolefin elastomer; φ, die land gap to die entrance gap ratio; PI, polydispersity index.

Figure 4: **Table 1** taken from [15], where the references also correspond to those of [15].

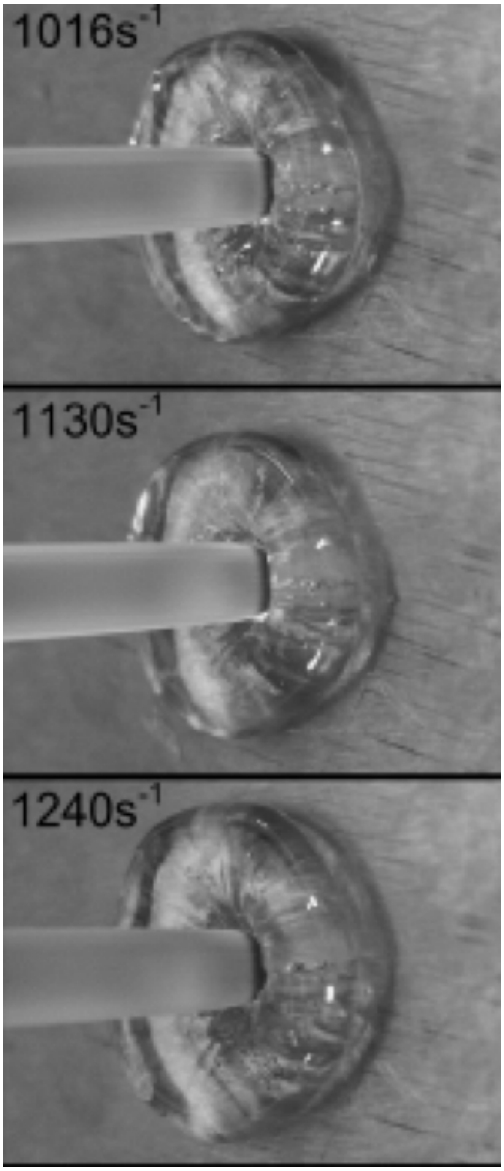

Figure 5: Images of die drool on a cylindrical die at shear rates of 1060 s^{-1}, 1130 s^{-1}, and 1240 s^{-1} taken from Video S1 of [16].

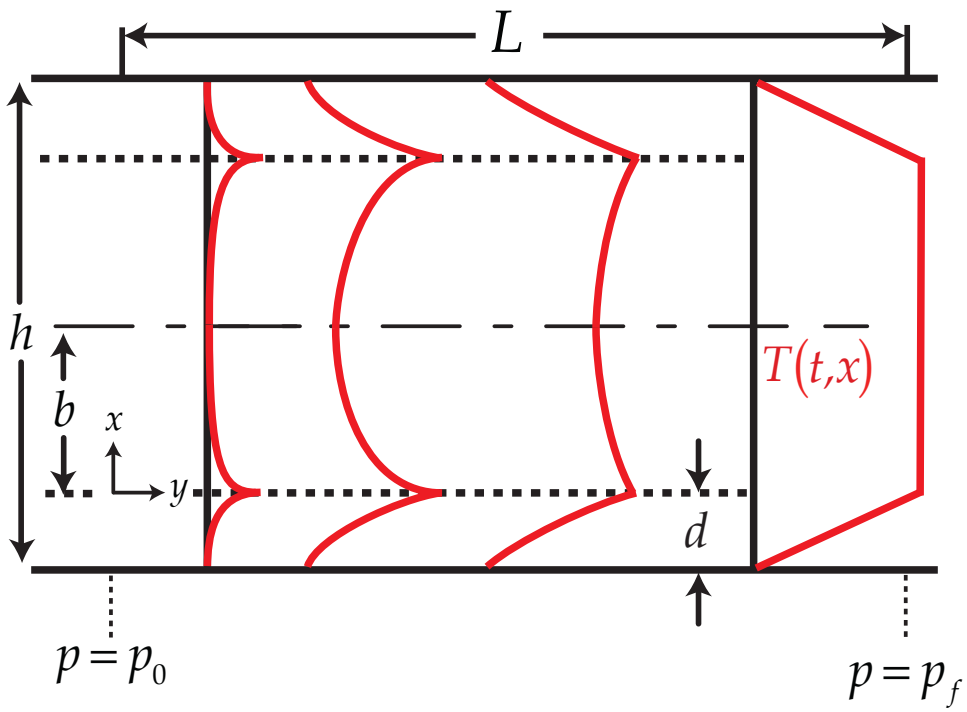

Figure 6: Evolving temperature profiles along die length.

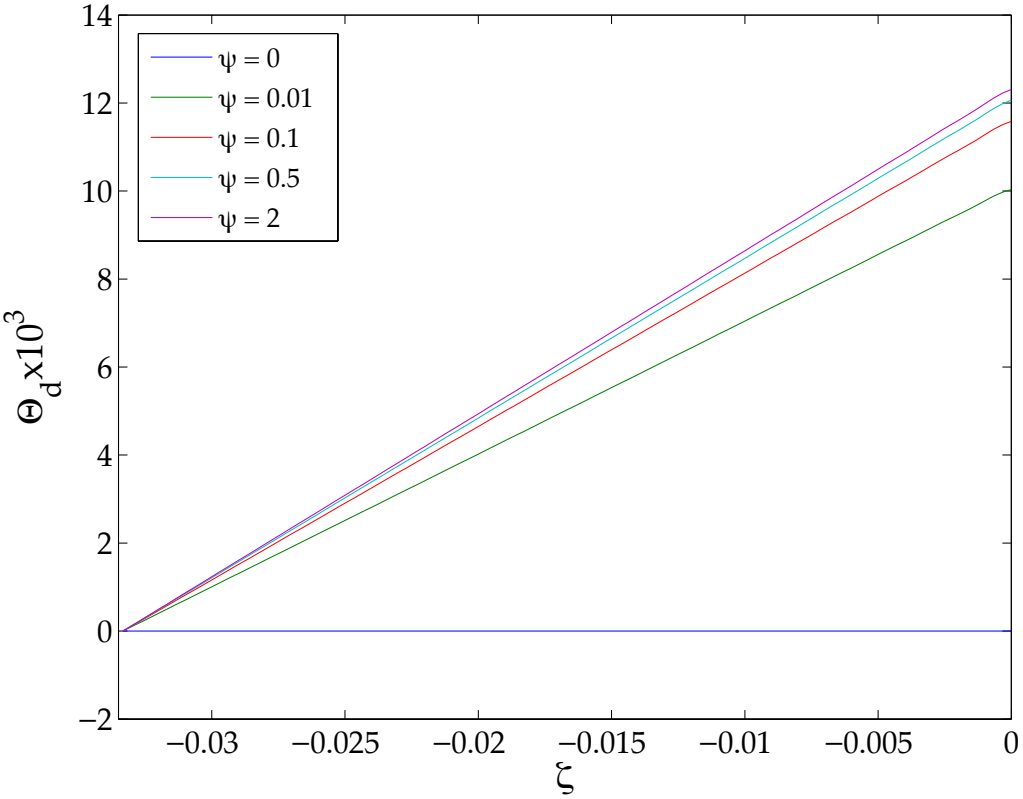

Figure 7: Dimensionless temperature rise in the drool layer calculated from Eq. (41).

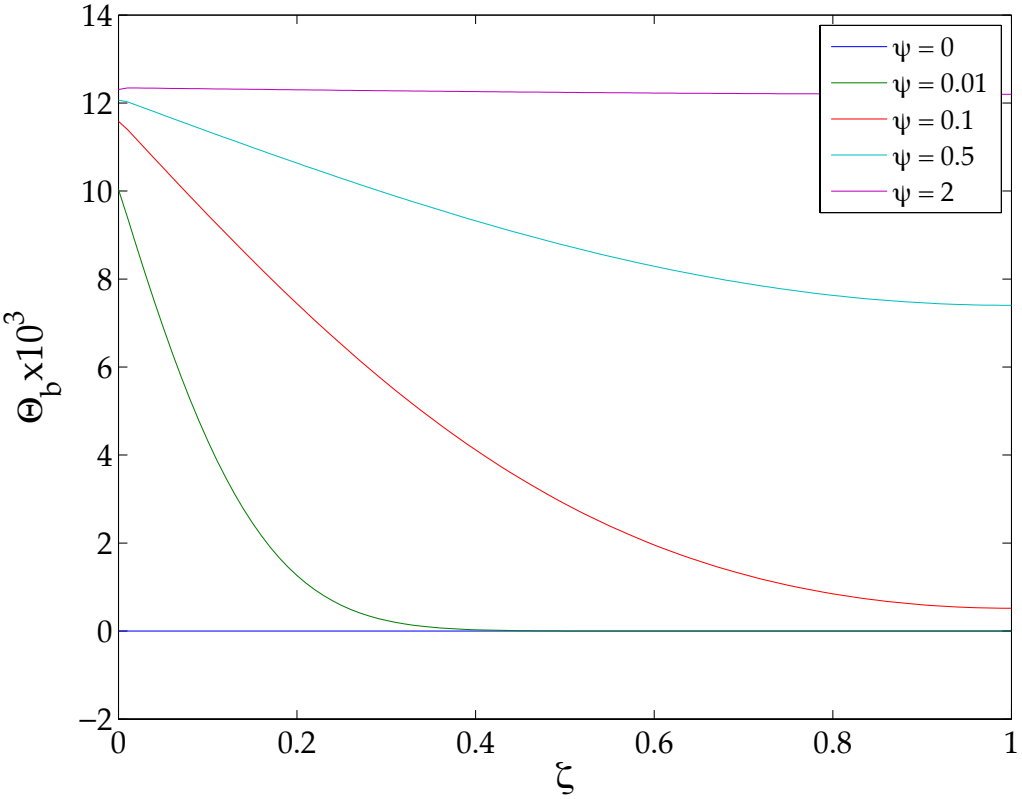

Figure 8: Dimensionless temperature rise in the bulk from Eq. (43).

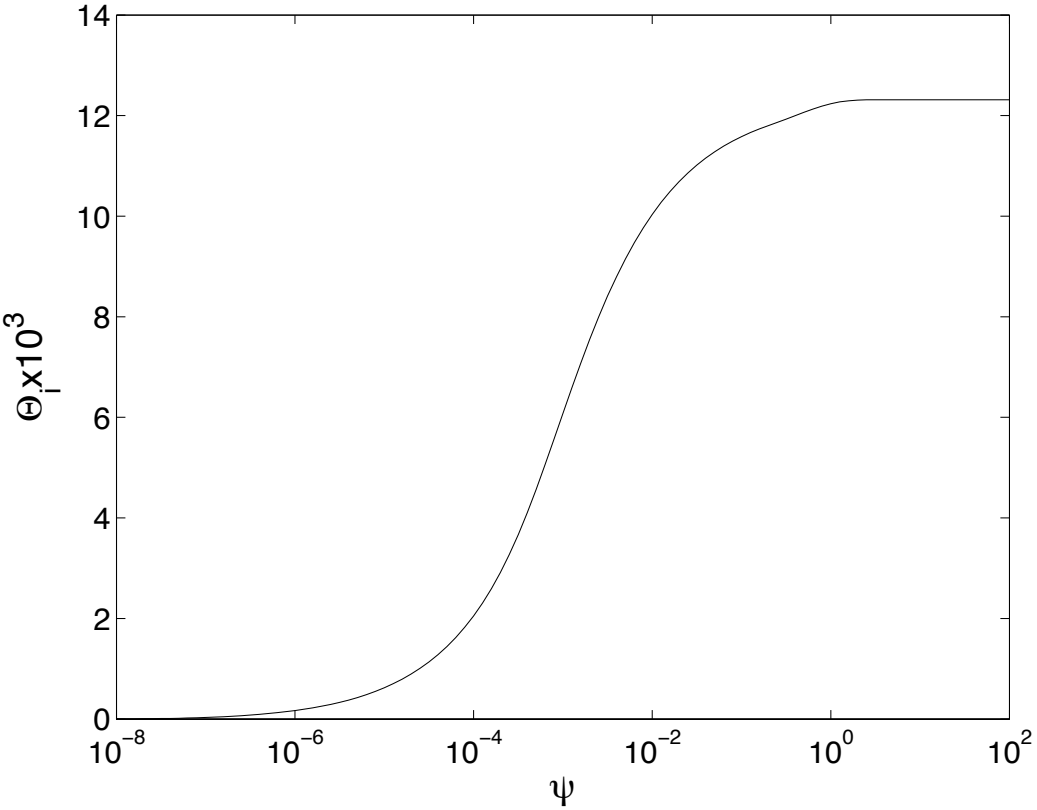

Figure 9: Dimensionless temperature rise at the slipping interface calculated from Eq. (44) showing knee in curve at $\psi \approx 0.01$.

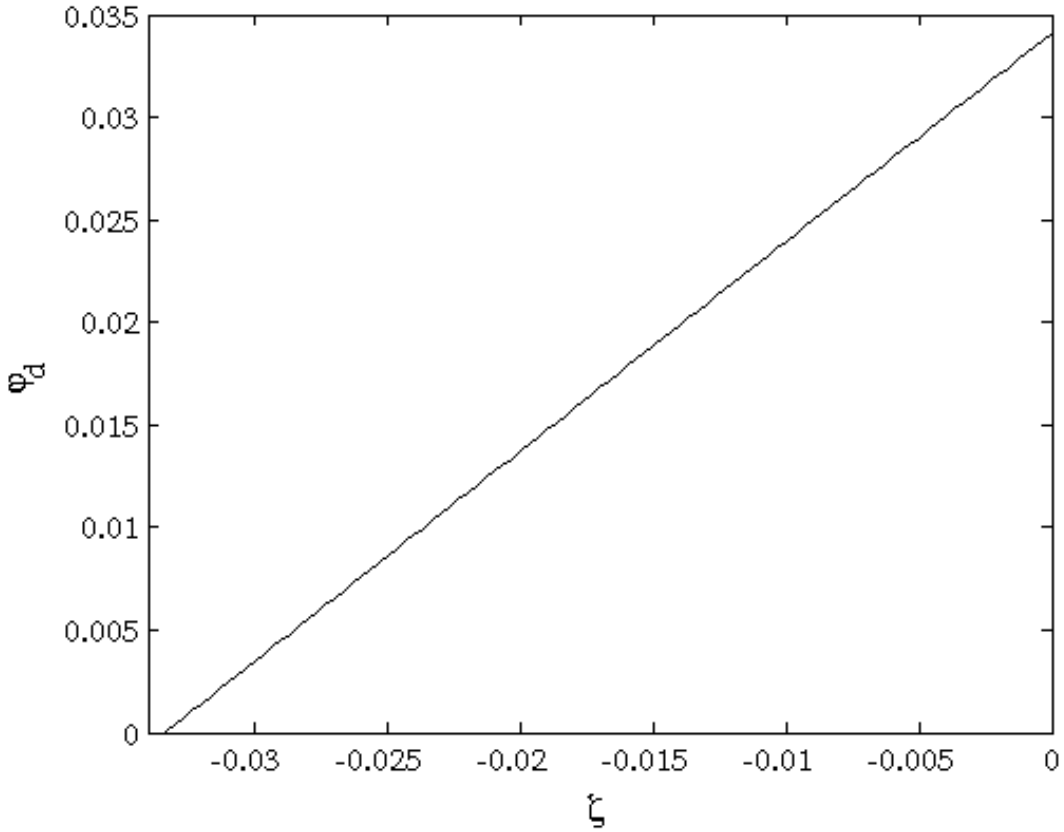

Figure 10: Dimensionless velocity profile in the drool layer for temperature-dependent Newtonian viscosity from Eq. (56).

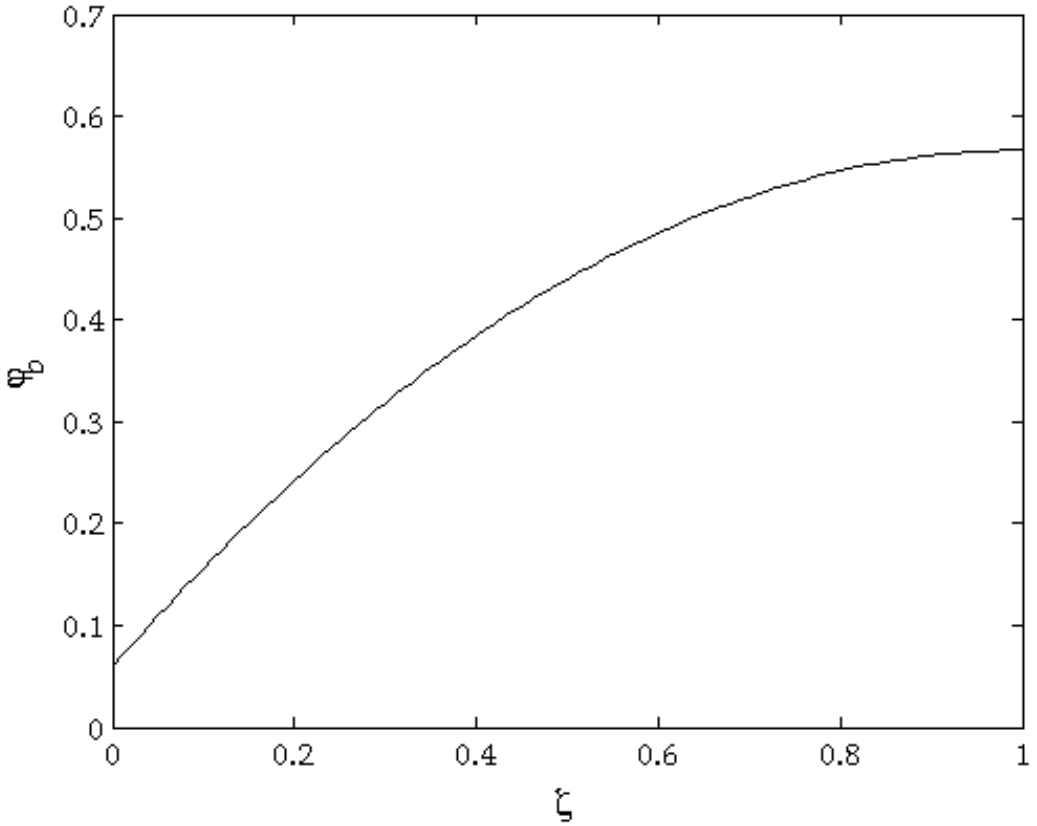

Figure 11: Dimensionless velocity profile in the bulk for temperature-dependent Newtonian viscosity from Eq. (58).

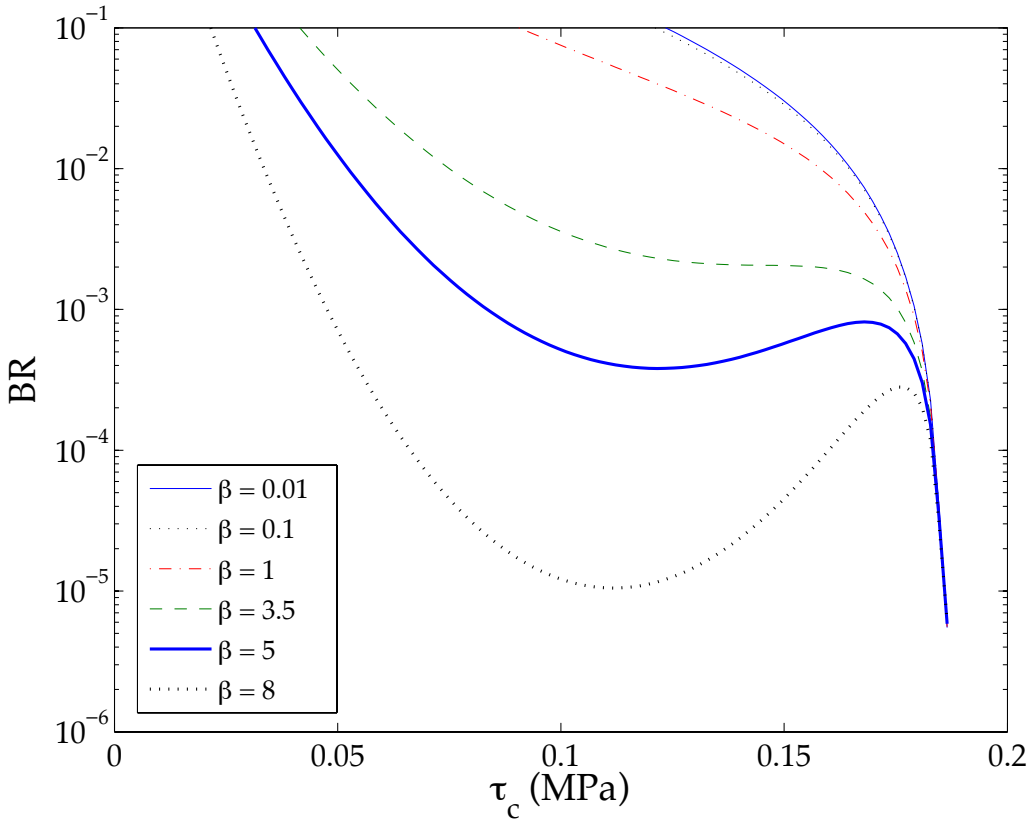

Figure 12: Semi-log plot showing non-monotonicity of buildup ratio *versus* dimensionless cohesive fracture strength arising in curves of high temperature-sensitivity, $\beta \geq 3.5$, where $BR\left(a,\varphi_s,\beta,F,\psi\right) = BR\left(a,0.0344,1.00,F,\psi\right)$.

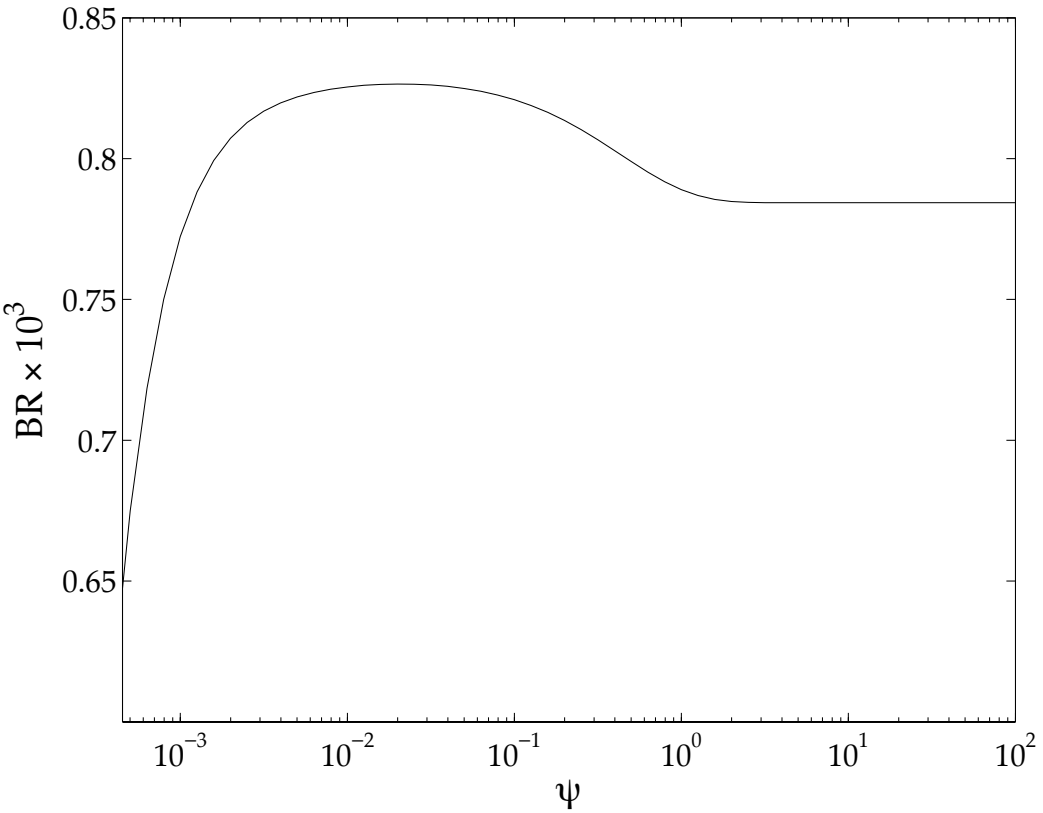

Figure 13: Semi-log plot showing buildup ratio versus dimensionless time for Worked Example 3, where
$BR\left(a,\varphi_s,\beta,F,\psi\right)=BR\left(0.0333,0.0344,1.00,0.371,\psi\right)$.

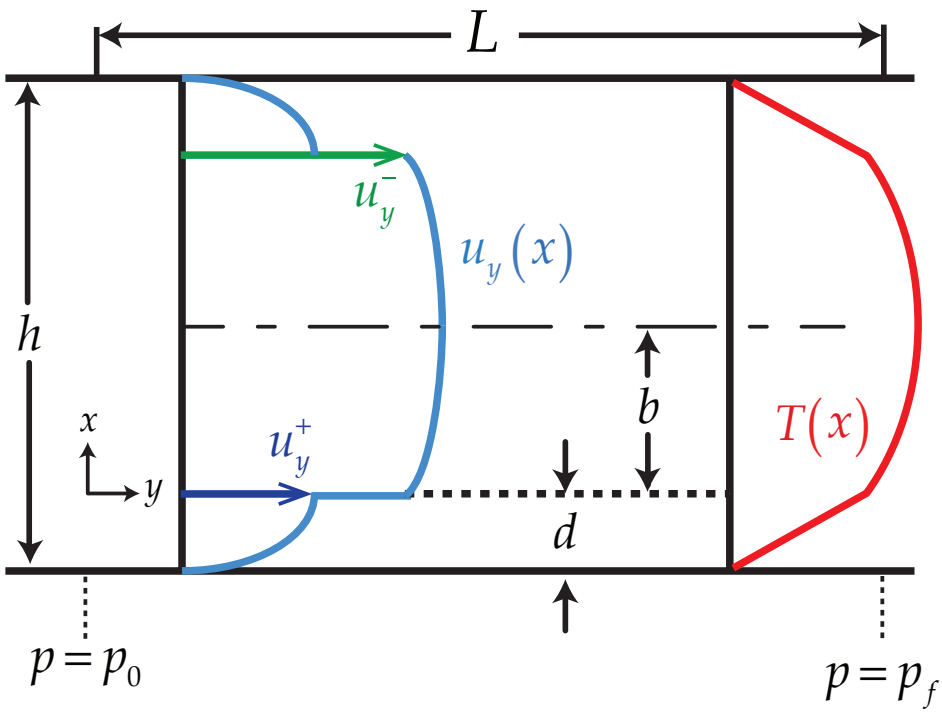

Figure 14: Velocity profiles and concomitant steady temperature profiles for the drool and bulk layers, where $u_s \equiv u_y^- - u_y^+$.

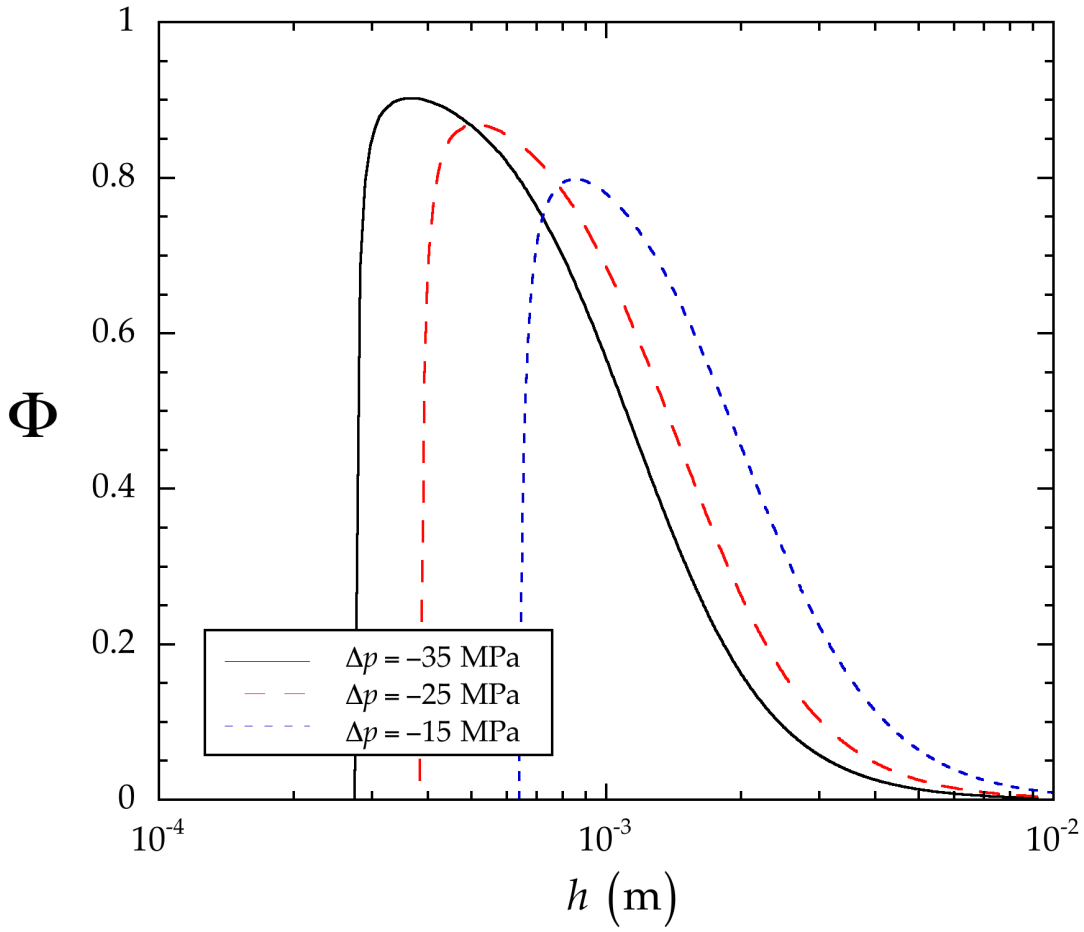

Figure 15: Slip heating to total heating ratio, Φ, as a function gap at three pressure drops, where all other properties are held constant, $\Phi\left(\Delta p, h, \mu, u_s, L, \tau_c\right) = \Phi\left(\Delta p, h, 600 \text{ Pa-s}, 200 \text{ mm/s}, 40 \text{ mm}, 0.12 \text{ MPa}\right)$.

Chapter 3. Adhesive Slip Heating

When plastic is extruded, the upper limiting throughput is often dictated by fine irregular distortions of the extrudate surface. Called *sharkskin melt fracture*, plastics engineers spike plastics formulations with processing aids to suppress these distortions. Sharkskin melt fracture is not to be confused with *gross melt fracture*, a larger scale distortion arising at throughputs higher than the critical throughput for sharkskin melt fracture ([19,31,32]; see Section 2.3.1 of [20]). Sharkskin melt fracture has been attributed to a breakdown of the no slip boundary condition in the extrusion die, that is, adhesive failure at the die walls, where the fluid moves with respect to the wall and is called *stick-slip* ([19], see Section 6.2.1 of [33];[23]).

Wall slip, or adhesive slip, occurs when a critical shear stress is exceeded at the extruder wall (see Figure 16) [23]. The slip speed is a function of wall shear stress and melt temperature, where a master curve of slip speed *versus* shear stress can be developed using Arrhenius shift factors. An analysis of the Arrhenius shift resulted in a master curve that neglected any heating caused by the slip or the viscous nature of the polymer [34,35,36,22]. For an analysis of the role of cohesive slip heating in die drool see [5,30]. By *die drool*, we mean the accumulation of unwanted material on the open faces of a plastics extrusion die. In this paper, we account for the frictional heating at the adhesive slip interface, which we call *slip heating*. Accurate slip speed prediction can help chemical engineers design dies that minimize undesirable slip related phenomena, such as melt fracture.

We derive an analytical solution for the steady temperature profiles in the extruder wall and in the bulk melt (see Figure 16), and we then investigate how

slip heating affects slip speed shift factors.

We focus on slit flow, which is used for film casting, sheet extrusion, curtain coating, and in many other unit operations. Specifically, we present the solutions for heat transfer in simple shear and pressure-driven slit flows subject to constant heat generation at the adhesive slip interface. We solve the energy equation in Cartesian coordinates for steady temperature profiles in the metal plate and polymer melt, when viscous dissipation is negligible, and when viscous heating is important. For this simplest relevant non-isothermal problem, we neglect convective heating in the melt and we model viscosity as a constant. We conclude by providing two worked examples showing the relevance of slip heating in flows with adhesive slip.

3.1. Method

For pressure-driven slit flow, we begin with the y – component of the dimensional equation of motion written in terms of the extra stress tensor (Eq. (B.5-2) of [24]):

$$\rho\left(\frac{\partial v_y}{\partial t}+v_x\frac{\partial v_y}{\partial x}+v_y\frac{\partial v_y}{\partial y}+v_z\frac{\partial v_y}{\partial z}\right)=-\frac{\partial p}{\partial y}-\left[\frac{\partial \boldsymbol{\tau}_{xy}}{\partial x}+\frac{\partial \boldsymbol{\tau}_{yy}}{\partial y}+\frac{\partial \boldsymbol{\tau}_{zy}}{\partial z}\right]+\rho g_y \tag{126}$$

which reduces to:

$$0=-\frac{dp}{dy}-\frac{d\boldsymbol{\tau}_{xy}}{dx} \tag{127}$$

for steady flow. Substituting Newton's law of viscosity:

$$\boldsymbol{\tau}_{xy}=-\mu\frac{dv_y}{dx} \tag{128}$$

into Eq. (12), we obtain the velocity dependent expression:

$$0 = -\frac{dp}{dy} + \mu \frac{d^2 v_y}{dx^2} \tag{129}$$

For polymers, when the molecular weight falls below the critical value for entanglement, the fluid behavior is nearly Newtonian. This often applies to commercial grades of condensation polymers such as polyamides, polyesters, and polycarbonates. Integrating Eq. (14) over y yields:

$$\frac{\Delta p}{L} = \mu \frac{d^2 v_y}{dx^2} \tag{130}$$

Inserting the dimensionless quantities from Table 2 into Eq. (15) produces the dimensionless velocity profile:

$$1 = -\frac{d^2 \varphi}{d\xi^2} \tag{131}$$

For simple shear between sliding plates, the y – component of the dimensional equation of motion [Eq. (11)] reduces to:

$$\frac{d\tau_{xy}}{dx} = 0 \tag{132}$$

Substituting Eq. (13) into Eq. (132), we find:

$$\frac{d^2 v_y}{dx^2} = 0 \tag{133}$$

from which, using the dimensionless quantities from Table 2, we obtain:

$$\frac{d^2 \phi}{d\xi^2} = 0 \tag{134}$$

The dimensional equation of energy, in terms of heat flux, is (Eq. B.8-1 [24]):

$$\rho\hat{C}_p\left(\frac{\partial T}{\partial t}+v_x\frac{\partial T}{\partial x}+v_y\frac{\partial T}{\partial y}+v_z\frac{\partial T}{\partial z}\right)=-\left[\frac{\partial q_x}{\partial x}+\frac{\partial q_y}{\partial y}+\frac{\partial q_z}{\partial z}\right]-\left(\frac{\partial \ln\rho}{\partial \ln T}\right)_p\frac{Dp}{Dt}-\left(\boldsymbol{\tau}:\nabla\mathbf{v}\right) \tag{135}$$

where the viscous heating term reduces to (using Eq. A.7-1 (C) of [24]):

$$-\left(\boldsymbol{\tau}:\nabla\mathbf{v}\right)=-\tau_{yx}\frac{\partial v_y}{\partial x} \tag{136}$$

The only source of heat within the fluid is that of viscous dissipation, which decreases with wall slip. Of course, slip heating at the interface also contributes to the fluid temperature rise. Inserting Eq. (18) and the $x-$component of Fourier's law of heat conduction:

$$q_x=-k\frac{\partial T}{\partial x} \tag{137}$$

into Eq. (17), we get:

$$\rho\hat{C}_p\left(\frac{\partial T}{\partial t}+v_x\frac{\partial T}{\partial x}+v_y\frac{\partial T}{\partial y}+v_z\frac{\partial T}{\partial z}\right)=k\left[\frac{\partial^2 T}{\partial x^2}+\frac{\partial^2 T}{\partial y^2}+\frac{\partial^2 T}{\partial z^2}\right]-\left(\frac{\partial \ln\rho}{\partial \ln T}\right)_p\frac{Dp}{Dt}-\tau_{yx}\frac{\partial v_y}{\partial x} \tag{138}$$

Evaluating Eq. (20) for constant ρ and inserting Eq. (13), we find:

$$\rho\hat{C}_p\left(\frac{\partial T}{\partial t}+v_x\frac{\partial T}{\partial x}+v_y\frac{\partial T}{\partial y}+v_z\frac{\partial T}{\partial z}\right)=k\left[\frac{\partial^2 T}{\partial x^2}+\frac{\partial^2 T}{\partial y^2}+\frac{\partial^2 T}{\partial z^2}\right]+\mu\frac{\partial v_y}{\partial x}\frac{\partial v_y}{\partial x} \tag{139}$$

At steady state, Eq. (21) reduces to:

$$\rho_f\hat{C}_{p,f}v_y\frac{\partial T_f}{\partial y}=k_f\frac{\partial^2 T_f}{\partial x^2}+\mu\frac{\partial v_y}{\partial x}\frac{\partial v_y}{\partial x} \tag{140}$$

Inserting the dimensionless groups from Table 2 into Eq. (22), we obtain:

$$\phi\mathrm{Pé}\frac{\partial\Theta}{\partial\varsigma}=\frac{\partial^2\Theta}{\partial\xi^2}+\mathrm{Br}\frac{\partial\varphi}{\partial\xi}\frac{\partial\varphi}{\partial\xi} \tag{141}$$

where:

$$\text{Pé} \equiv \frac{v_{\max} b^2}{\alpha_f L} \tag{142}$$

and:

$$\text{Br} \equiv \frac{\mu}{k_f T_0}\left(\frac{b^2 \Delta P}{L\mu}\right)^2 = \frac{\tau_c^4 L^2}{k_f T_{0,f} \mu \left(\Delta P\right)^2} \tag{143}$$

for pressure-driven flow. We develop a similar differential equation for flow in simple shear:

$$\phi \text{Pé} \frac{\partial \Theta}{\partial \varsigma} = \frac{\partial^2 \Theta}{\partial \xi^2} + \text{Br} \frac{\partial \phi}{\partial \xi} \frac{\partial \phi}{\partial \xi} \tag{144}$$

where:

$$\text{Pé} \equiv \frac{v_w b^2}{\alpha_f L} \tag{145}$$

and:

$$\text{Br} = \frac{\mu v_w^2}{T_0 k_f} \tag{146}$$

The convective heating terms in Eqs. (23) and (144) can be neglected when:

$$\text{Pé} \ll 1 \tag{147}$$

Additionally, from Eqs. (23) and (144), we learn that:

$$\text{Br} \ll 1 \tag{148}$$

is a sufficient condition for accurately neglecting viscous dissipation for the slit flow of Newtonian fluids. For non-Newtonian fluids, Eq. (24) can be reformulated following the method outlined in Table 4.4-1 of [25].

For slip heating, we can arrive at a second sufficient condition by comparing the heat flux from the slipping interface to the viscous heating. This yields the dimensionless group:

$$\mathrm{Gi} \equiv \frac{\mu b}{u_s \tau_{yx}\Big|_{x=0}} \left[\frac{\partial v_y}{\partial x}\right]^2 = \frac{\mu b}{u_s \tau_c} \left[\frac{\partial v_y}{\partial x}\right]^2 \tag{149}$$

where, by definition, the fluid cohesive fracture strength, τ_c, is equal to the shear stress at the slipping interface. Eq. (30) implies that $\mathrm{Gi} \ll 1$ is a second sufficient condition for accurately neglecting viscous dissipation. For non-Newtonian fluids, Eq. (30) must be reformulated. For pressure-driven capillary flow, an interesting recent study includes adhesive slip and viscous heating, but neglects slip heating (see Eqs. (2)-(6) of [26].

3.2. Results: Steady Temperature Rise Without Viscous Dissipation

When viscous dissipation and convective heating can be neglected, Eq. (23) reduces to:

$$\frac{\partial^2 \Theta_f}{\partial \zeta^2} = 0 \tag{150}$$

for pressure driven flow in the polymer melt. We find a similar expression for the metal wall:

$$\frac{\partial^2 \Theta_m}{\partial \zeta^2} = 0 \tag{151}$$

Eqs. (150) and (151) are solved subject to the following boundary conditions at the adiabatic mid-plane:

$$\left.\frac{d\Theta_f}{d\zeta}\right|_{\zeta=1} = 0 \tag{152}$$

at the slipping interface:

$$\Theta_m(0) = \Theta_f(0) \tag{153}$$

$$K \left. \frac{d\Theta_m}{d\zeta} \right|_{\zeta=0} - \left. \frac{d\Theta_f}{d\zeta} \right|_{\zeta=0} = F \tag{154}$$

where:

$$K = \frac{k_m}{k_f} \tag{155}$$

and at the isothermal plate exterior:

$$\Theta_m(-a) = \Theta_w \tag{156}$$

where the plate is normally immersed in a bath. We find the dimensionless temperature profile for the polymer melt:

$$\Theta_f = \frac{Fa}{K} + \Theta_w \tag{157}$$

where Θ_w is the plate exterior temperature. We also obtain the plate temperature profile:

$$\Theta_m = \frac{F}{K}(\zeta + a) + \Theta_w \tag{158}$$

Substituting the dimensional expressions from Table 1 into Eqs. (157) and (158), we recover the dimensional temperature profiles for the polymer melt and plate:

$$T_f = \frac{\tau_c u_s d}{k_m} + T_w \tag{159}$$

$$T_m = \frac{\tau_c u_s}{k_m}(x + d) + T_w \tag{160}$$

which the plastics engineer can use to adjust observed temperatures for slip heating effects during rheometry experiments. Eqs. (159) and (160) are accurate when both convection and viscous dissipation may be neglected, and they are

applicable to pressure-driven and simple shear flows. Eq. (159) is one of two main results of this paper.

3.3. Results: Steady Temperature Rise With Viscous Dissipation

For many polymers, viscous dissipation is an important contribution to heating during extrusion and other processes. We evaluate the contribution of viscous dissipation in addition to slip heating for pressure-driven and simple shear flows.

3.3.1. Pressure-Driven Flow

When convective heating is neglected, Eq. (23) reduces to:

$$0 = \frac{\partial^2 \Theta_f}{\partial \xi^2} + \mathrm{Br}\left(\frac{\partial \varphi}{\partial \xi}\right)^2 \tag{161}$$

for the polymer melt subjected to pressure-driven flow, where viscous dissipation is important. Evaluation of Eq. (131) subject to the boundary conditions at the slipping metal-polymer interface:

$$\varphi(0) = \varphi_s \tag{162}$$

and the polymer mid-plane:

$$\left.\frac{d\varphi}{d\xi}\right|_{\xi=1} = 0 \tag{163}$$

yields:

$$\varphi(\xi) = \xi - \frac{\xi^2}{2} + \varphi_s \tag{164}$$

which is the velocity profile for a polymer having constant viscosity under pressure-driven flow between two plates.

Taking the derivative of Eq. (164):

$$\frac{d\varphi}{d\zeta} = 1 - \zeta \tag{165}$$

and inserting into Eq. (161), we find:

$$\frac{d^2\Theta_f}{d\zeta^2} = -\mathrm{Br}\left(1-\zeta\right)^2 = -\mathrm{Br}\left(\zeta^2 - 2\zeta + 1\right) \tag{166}$$

We evaluate Eq. (166) using the boundary conditions in Eqs. (152) - (156) and obtain:

$$\Theta_f\left(\zeta\right) = -\mathrm{Br}\left(\frac{\zeta^4}{12} - \frac{\zeta^3}{3} + \frac{\zeta^2}{2}\right) + \frac{\mathrm{Br}}{3}\zeta + a\left(\frac{F}{K} + \frac{\mathrm{Br}}{3K}\right) + \Theta_w \tag{167}$$

the dimensionless polymer melt temperature profile. Similarly, we find:

$$\Theta_m\left(\zeta\right) = \left(\frac{F}{K} + \frac{\mathrm{Br}}{3K}\right)\left(\zeta + a\right) + \Theta_w \tag{168}$$

which is the dimensionless plate temperature profile. When $\mathrm{Br} \ll 1$, we recover Eqs. (157) and (158) from Eqs. (167) and (168). Eqs. (167) and (168) can be used to correct rheological measurements for slip heating with viscous dissipation during pressure-driven flow between two plates.

3.3.2. Simple Shearing Flow

Eq. (144) reduces to:

$$\frac{d^2\Theta_f}{d\zeta^2} = -\mathrm{Br}\left(\frac{d\phi}{d\zeta}\right)^2 \tag{169}$$

when convective heating in the polymer melt is neglected, $\mathrm{Pé} \ll 1$, and viscous dissipation is included. We develop the melt velocity profile by evaluating Eq. (134) subject to the boundary conditions at the slipping plate-melt interfaces:

$$\phi(0) = 1 - \phi_s \tag{170}$$

$$\phi(2) = \phi_s \tag{171}$$

where $\zeta = 0$ corresponds to the interface between the melt and the moving plate and ϕ_s is the slip speed. We find the velocity profile:

$$\phi(\zeta) = \frac{2\phi_s - 1}{2}\zeta + 1 - \phi_s \tag{172}$$

for the polymer melt and substitute the derivative of Eq. (172):

$$\frac{d\phi}{d\zeta} = \frac{2\phi_s - 1}{2} \tag{173}$$

into Eq. (169) to obtain:

$$\frac{d^2\Theta_f}{d\zeta^2} = -\mathrm{Br}\left(\frac{2\phi_s - 1}{2}\right)^2 \tag{174}$$

which is the differential temperature profile in terms of slip velocity. Integrating this ordinary differential equation using the boundary conditions in Eqs. (152) - (156), we find:

$$\Theta_f(\zeta) = \frac{\mathrm{Br}(2\phi_s - 1)^2}{8}\zeta^2 + \frac{\mathrm{Br}(2\phi_s - 1)^2}{4}\zeta + a\left(\frac{F}{K} + \frac{\mathrm{Br}(2\phi_s - 1)^2}{4K}\right) + \Theta_w \tag{175}$$

which is the dimensionless melt temperature profile in simple shear with viscous dissipation. Similarly, we solve for the dimensionless plate temperature profile:

$$\Theta_m(\zeta) = \left(\frac{F}{K} + \frac{\mathrm{Br}(2\phi_s - 1)^2}{4K}\right)(\zeta + a) + \Theta_w \tag{176}$$

The interfacial temperature at the moving plate is obtained by setting $\zeta = 0$ in Eq. (176):

$$\Theta_i = \left(\frac{F}{K} + \frac{\mathrm{Br}\left(2\phi_s - 1\right)^2}{4K} \right) a + \Theta_w \tag{177}$$

which the rheologist can use to correct observed temperature at the slipping interface for slip heating and viscous dissipation during simple shearing flow. Since polymer viscosity often has an Arrhenius temperature dependence, our solutions could be improved by including this in our calculation. However, complexity of this level is outside the scope of discussion presented here. Eqs. (177) along with (159) are the main results of this paper. The following worked examples demonstrate the usefulness of these results.

3.4. Worked Example 1: Correcting wall slip data for slip heating

A rheologist would like to adjust slip speed *versus* shear stress data collected using a sliding plate rheometer. The data, provided by [34], were recorded for four different temperatures using magnetic 420 stainless steel plates and HDPE 56B\3830 resin and are presented in Figure 17. He would also like to create a master curve of slip speed *versus* shear stress for all temperatures using Arrhenius shift factors. A master curve for the data is available in [35] without consideration of slip heating effects (see Figure 8).

He first calculates the temperature adjustment for each slip speed and shear rate using Eq. (159). Correction increases the melt temperature by up to 5 K in the presence of slip heating which may contribute to thermal degradation (see Table 3). By inputting these corrected temperatures into the Arrhenius shift factor expression:

$$a_{T,s} = \exp\left[E_s\left(\frac{1}{T} - \frac{1}{T_r}\right)\right] \tag{178}$$

for $T_r = 473\,\mathrm{K}$ and $E_s = 4500.7\,\mathrm{K}$, he obtains a set of shift factors for each data point (see Table 3). Using these shift factors, he creates the master curve shown in Figure 9. He notices that the data at high shear rates, $\tau > 0.12$, collapse more effectively than those at low shear rates, $\tau < 0.12$. The data for the lowest temperature, $T = 145\,^{\circ}\mathrm{C}$, has a different slope from data at other temperatures both before and after adjustment which reduces the master curve fit. Additionally, the goodness of fit to a power-law function is unchanged for adjusted shift factors compared to the original shift factors presented in [35].

3.5. Worked Example 2: Correcting wall slip data for both slip heating and viscous dissipation

The rheologist examines the same system as before, but he would like to consider viscous dissipation in his analysis. He calculates the temperature adjustments for each data point using Eq. (177). Inclusion of viscous dissipation in conjunction with slip heating increases the temperature even further. However, the magnitude of temperature increase from viscous dissipation relative to temperature rise from slip heating varies with slip speed and wall shear stress. Figure 20 shows the fraction of total temperature rise attributed to slip heating *versus* wall shear stress and parameterized by exterior surface temperature. The temperature rise increases with exterior temperature, which increases wall slip. This increases the importance of slip heating at high

temperature and wall shear stress. Viscous dissipation contributes to temperature rise most at low temperature and wall shear stress. However, at any point between these to extremes, it is necessary to consider both viscous dissipation and slip heating.

The rheologist determines the shift factors from Eq. (178) (see Table 3) and produces the master curve shown in Figure 11. He also develops Figure 22, which compares the three different master curves on a single plot. Despite the difference in approach, the master curves collapse similarly with the same minor deviations from the Arrhenius form at low temperature, or low slip speed, measurements. The power-law curves for the slip heating temperature rise, with and without viscous dissipation, have similar values for the front factor and exponents, which is unexpected since there is a large difference in temperature rise when viscous dissipation is included.

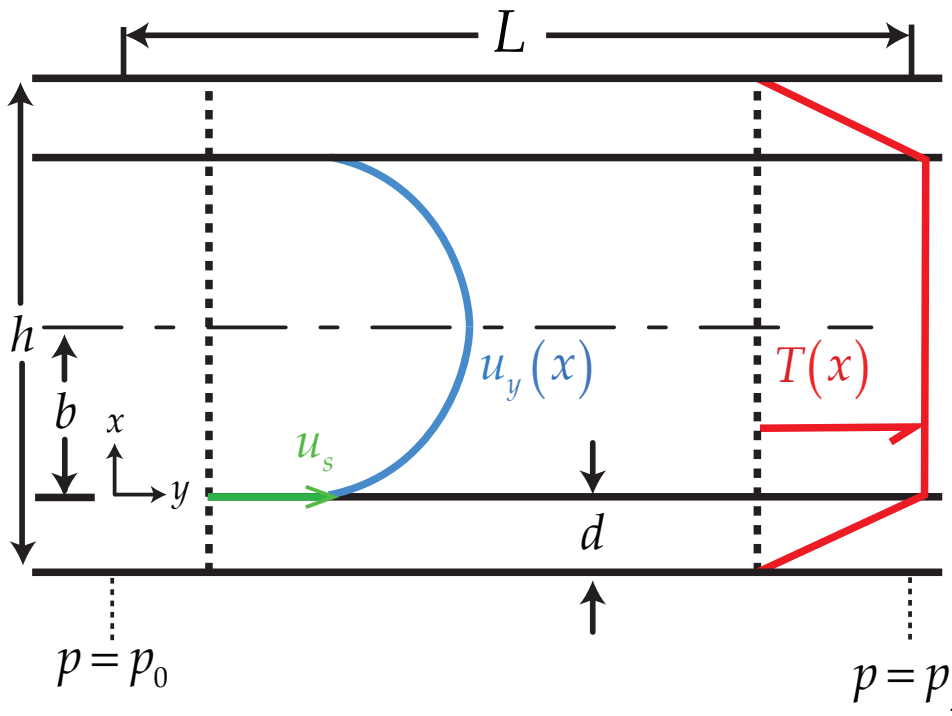

Figure 16: Velocity profiles and concomitant steady temperature profiles for pressure-driven flow with slip heating between the melt and the wall.

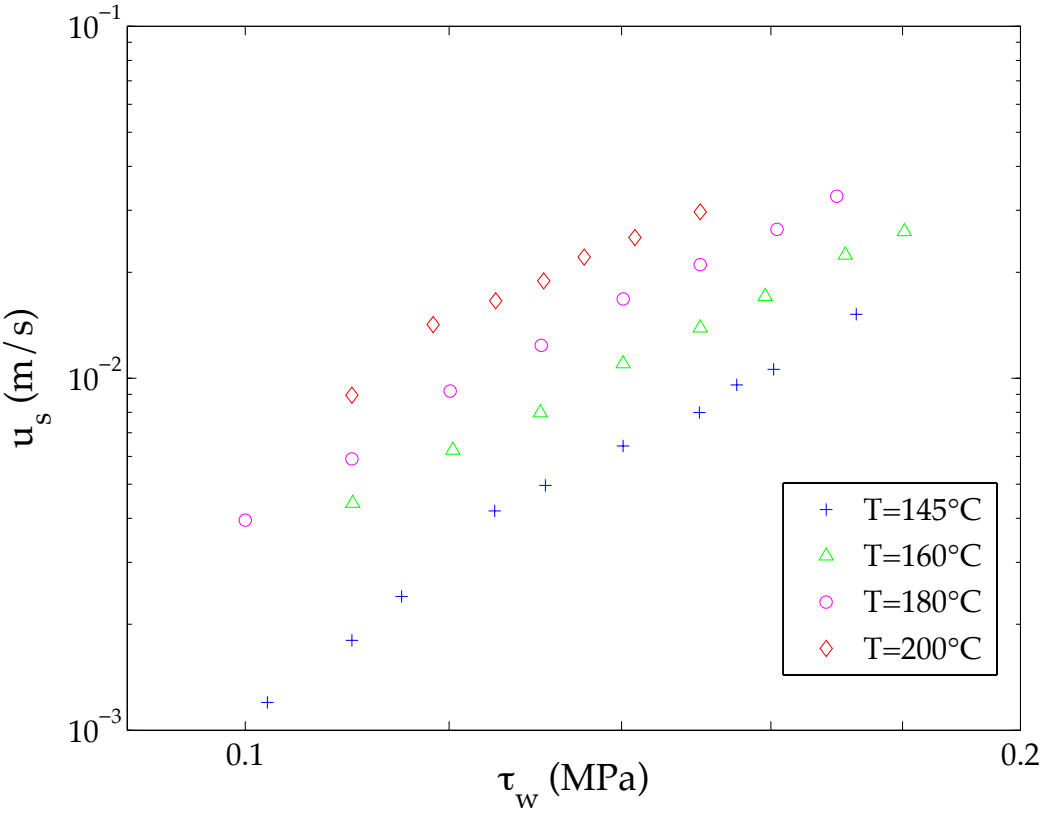

Figure 17: Slip speed *versus* wall shear stress measured at four temperatures (see FIG. 4 of [34]).

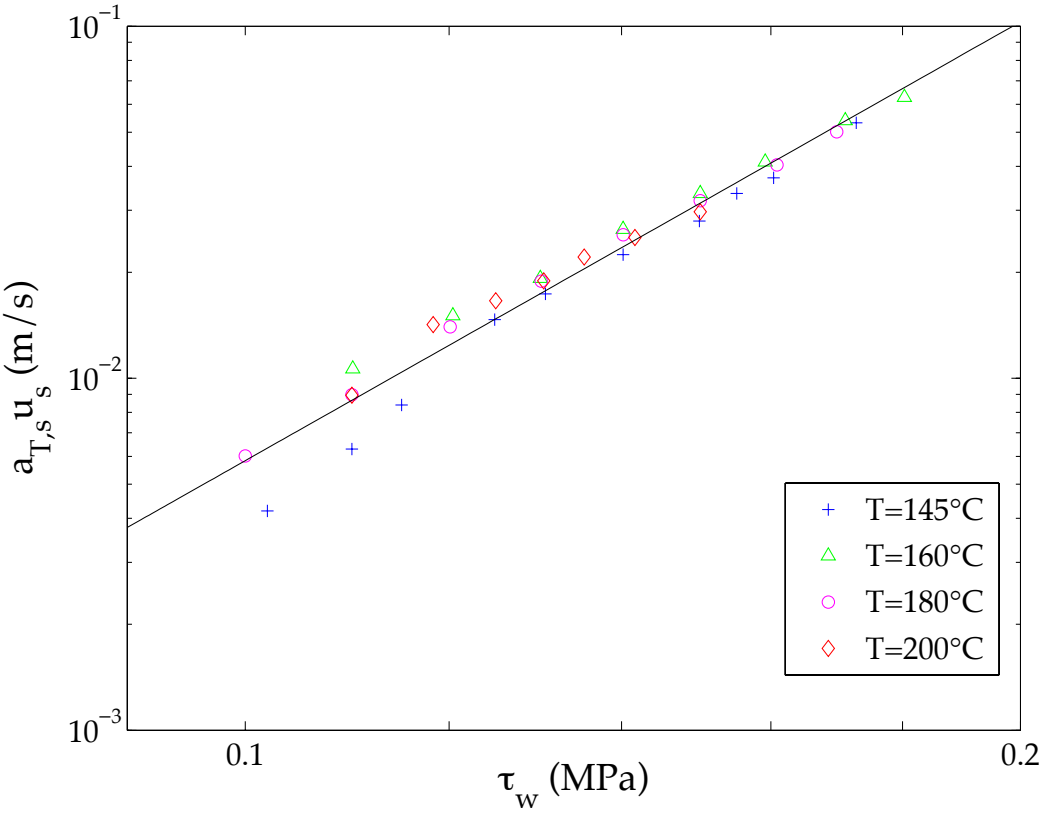

Figure 18: Shifted slip speed *versus* wall shear stress (see FIG. 17 of [35]) with power-law fit, $a_{T,s}u_s = 80.72\tau_w^{4.14}$.

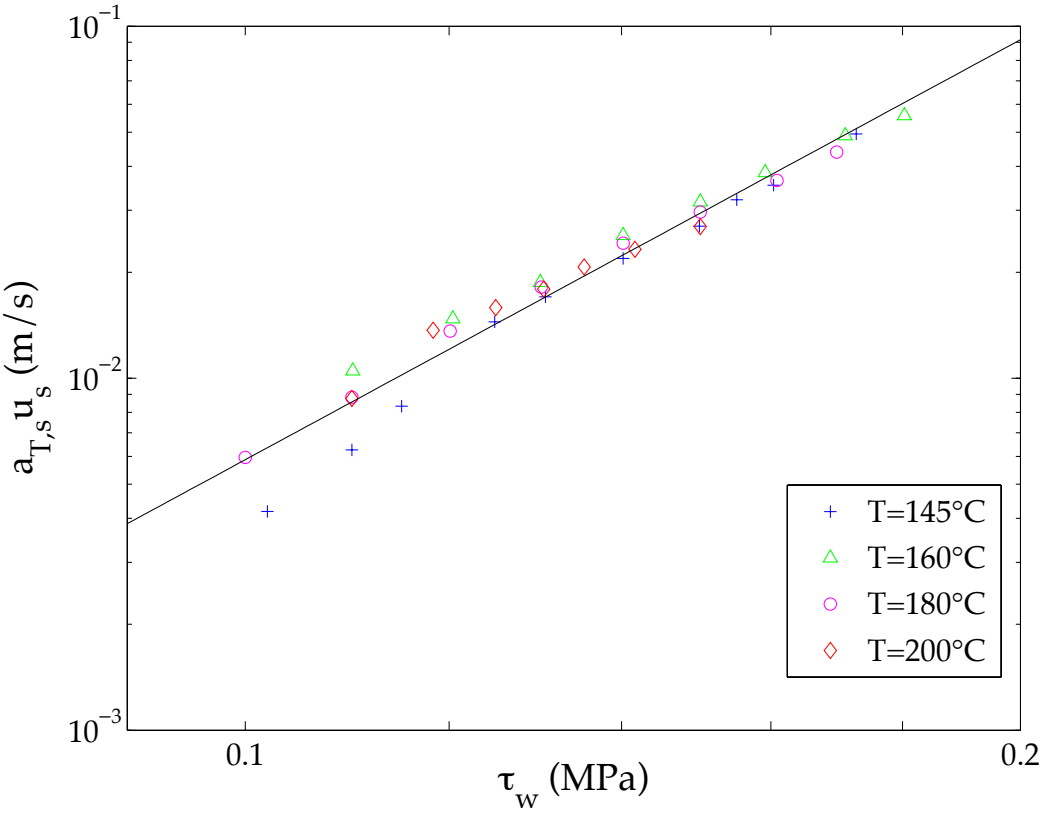

Figure 19: Shifted slip speed *versus* wall shear stress with temperature adjustment for slip heating having power law fit $a_{T,s}u_s = 53.96\tau_w^{3.96}$ (compare with $a_{T,s}u_s = 80.72\tau_w^{4.14}$ from uncorrected Figure 18).

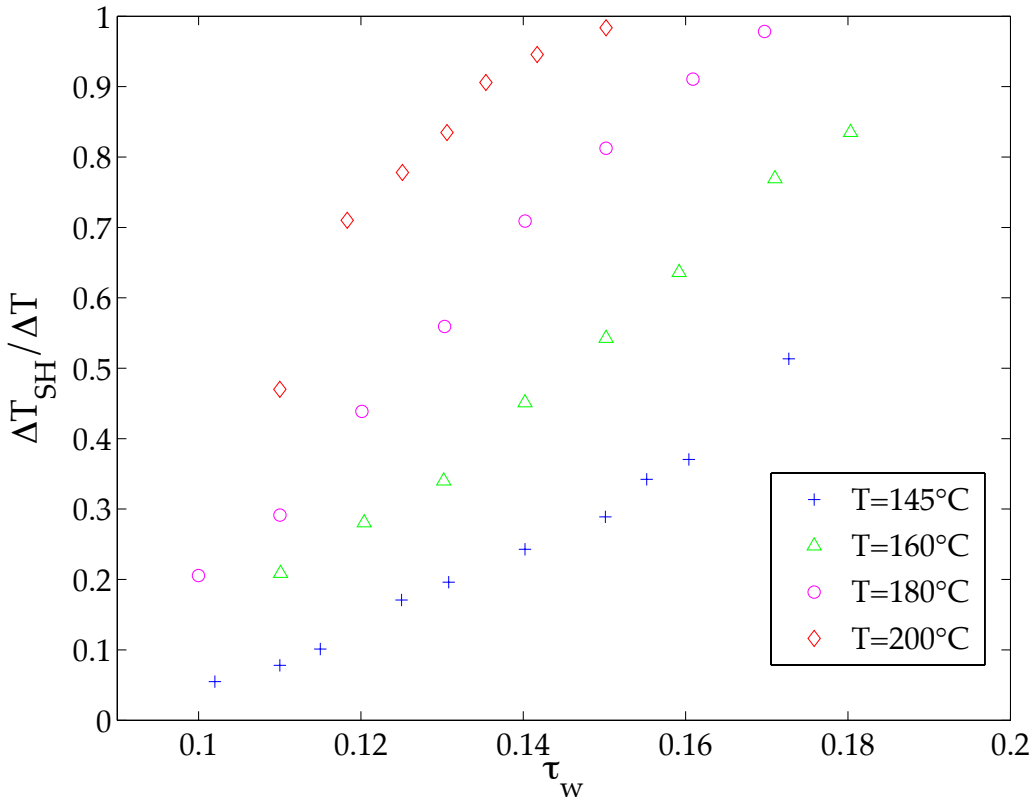

Figure 20: Temperature rise from slip heating as a fraction of total temperature rise from viscous dissipation plus slip heating *versus* wall shear stress.

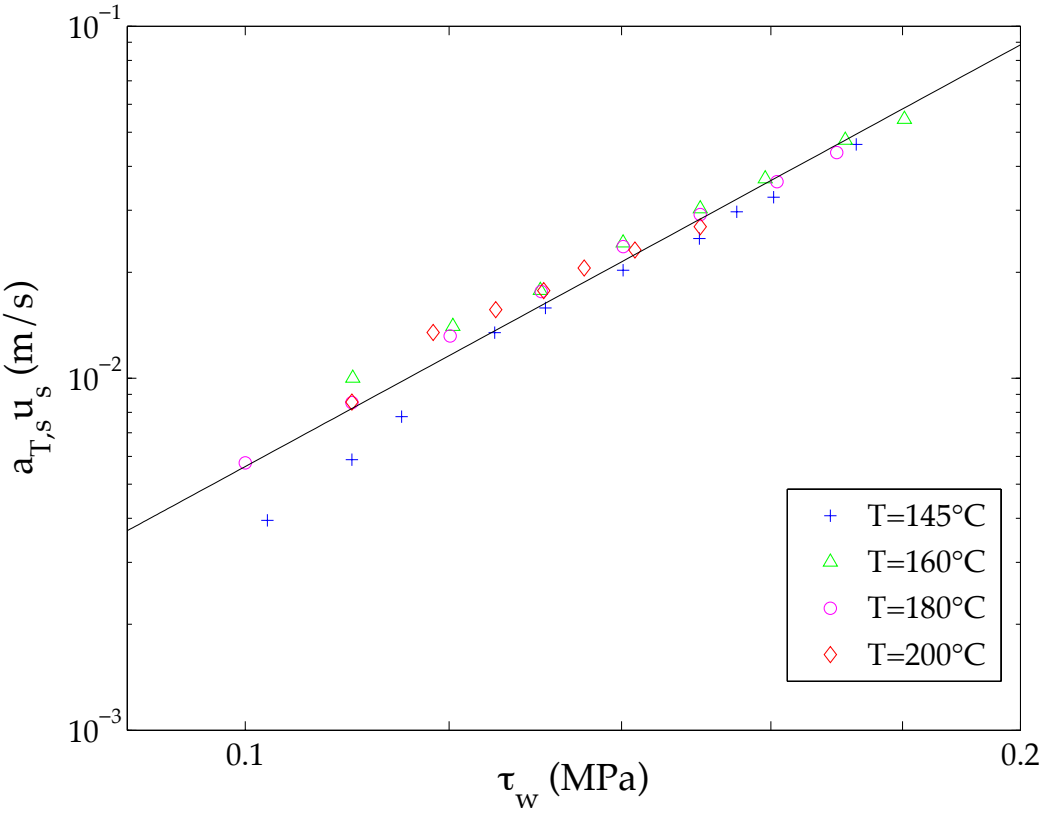

Figure 21: Shifted slip speed *versus* wall shear stress with temperature adjusted for slip heating and viscous dissipation having power law fit $a_{T,s}u_s = 53.51\tau_w^{3.98}$ (which closely matches $a_{T,s}u_s = 53.96\tau_w^{3.96}$ of Figure 19).

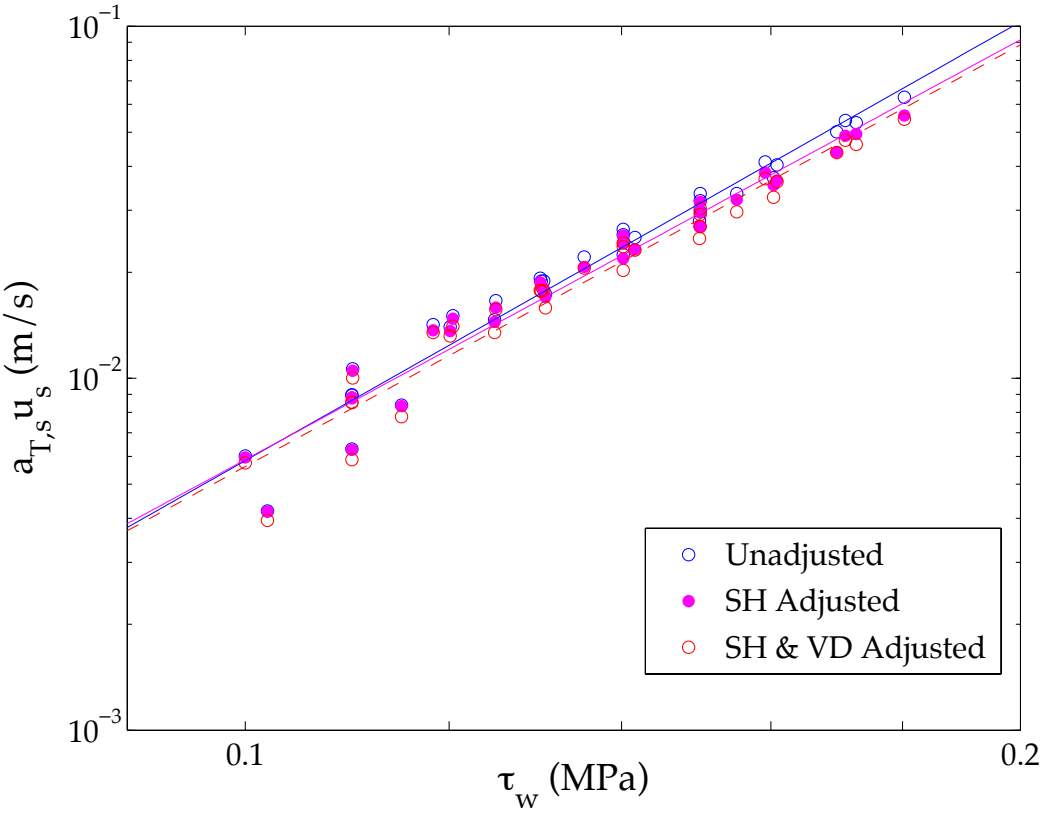

Figure 22: Shifted unadjusted (blue), slip heating adjusted (magenta, solid), and viscous dissipation adjusted (red, dashed) slip speed *versus* wall shear stress data and corresponding power-law fits.

Table 3: Temperature rises during slip heating with and without viscous dissipation and corresponding shift factors for slip data at different temperatures and wall shear stresses

$T_{meas} = 145°C$					$T_{meas} = 160°C$				
τ_w (MPa)	ΔT_{SH} (°C)	$a_{T,SH}$	ΔT_{SHVD} (°C)	$a_{T,SHVD}$	τ_w (MPa)	ΔT_{SH} (°C)	$a_{T,SH}$	ΔT_{SHVD} (°C)	$a_{T,SHVD}$
0.102	0.13	3.49	2.41	3.29	0.110	0.53	2.38	2.52	2.27
0.110	0.21	3.48	2.75	3.26	0.120	0.82	2.36	2.91	2.25
0.115	0.30	3.47	2.95	3.24	0.130	1.13	2.34	3.31	2.23
0.125	0.57	3.45	3.32	3.21	0.140	1.67	2.31	3.70	2.21
0.131	0.70	3.43	3.59	3.19	0.150	2.26	2.28	4.17	2.18
0.140	0.98	3.41	4.01	3.16	0.159	2.95	2.25	4.64	2.16
0.150	1.30	3.38	4.50	3.12	0.171	4.15	2.18	5.39	2.12
0.155	1.61	3.36	4.70	3.10	0.180	5.10	2.13	6.11	2.08
0.160	1.84	3.34	4.97	3.08					
0.173	2.84	3.25	5.54	3.04					
$T_{meas} = 180°C$					$T_{meas} = 200°C$				
τ_w (MPa)	ΔT_{SH} (°C)	$a_{T,SH}$	ΔT_{SHVD} (°C)	$a_{T,SHVD}$	τ_w (MPa)	ΔT_{SH} (°C)	$a_{T,SH}$	ΔT_{SHVD} (°C)	$a_{T,SHVD}$
0.100	0.43	1.51	2.08	1.45	0.110	1.07	0.98	2.27	0.96
0.110	0.70	1.50	2.41	1.44	0.118	1.82	0.96	2.56	0.95
0.120	1.20	1.48	2.73	1.43	0.125	2.25	0.96	2.89	0.94
0.130	1.75	1.47	3.13	1.42	0.131	2.67	0.95	3.20	0.94
0.140	2.55	1.44	3.60	1.41	0.135	3.24	0.94	3.58	0.93
0.150	3.42	1.41	4.20	1.39	0.142	3.85	0.93	4.07	0.92
0.161	4.62	1.38	5.07	1.36	0.150	4.83	0.91	4.91	0.91
0.170	6.05	1.34	6.18	1.33					

Chapter 4. Conclusion

We arrive at an expression for the die drool flow rate [Eq. (57)]. We also develop an expression for the highest temperature in the flow field [Eq. (44)], where the drool touches the bulk fluid. Since our temperature rise analysis at the cohesive slip interface neglects the effect of viscous heating, our temperature rise predictions from Eqs. (41), (43), (48) and (49) are conservative. The temperature dependent steady velocity profiles for slit flow were presented and used to determine the steady buildup ratio, which can be used by the plastics engineer to quantify drool. Thus, Eqs. (57), (59), and (60) are main results of this work. We expect these results to be accurate when $\mathrm{Gi} \ll 1$, $\mathrm{Br} \ll 1$, and at least one condition is satisfied in each pair of Eqs. (25)-(26) and Eqs. (27)-(28).

Buildup ratio increases with decreasing fluid fracture strength, as expected, since the bulk and drool layers can separate at lower shear stresses. Greater fluid thermal sensitivity can mitigate increasing buildup ratios in fluids with low cohesive fracture strengths by increasing the viscosity difference between the two layers. When a material is highly sensitive to temperature ($\beta > 35$), the buildup ratio monotonicity is lost, which may explain the difficulty in troubleshooting flows with large buildup ratios. Figure 13 shows that long operation times also reduce die lip buildup and is an important result of this work. These results are accurate for the sufficient condition where ψ is not $\ll 1$.

Many attribute drool to the shear-induced mass transfer of low molecular weight species toward the wall [9,10,12,28]. Our work includes this possibility as a special case. For instance, when the die drool is found to have a lower molecular weight than the bulk [13], we think this is probably caused by polymer

thermal degradation through scission (such as is common for polypropylene), and specifically, when the temperature given by Eq. (44) exceeds the degradation point for the polymer.

Slip heating and viscous dissipation must both be considered in temperature analysis of drooling systems. Eq. (124) is a main result of this work and should be used to determine when one or the other can be neglected. When $\Phi \approx 0$, slip heating may be excluded. When $\Phi \approx 1$, viscous dissipation should be neglected, and Eqs. (43) and (44) of [5] become appropriate choices for thermal analysis. However, when $0 \ll \Phi \ll 1$, neither heating source may be neglected, and Eqs. (109) and (110) of this work should be used. Eq. (111) is the other main result, and it is used to determine the maximum temperature rise in the polymer. Plastics processors must ensure that this temperature rise falls below the degradation point of the polymer melt.

We develop expressions for correcting melt temperatures in flows with wall slip where viscous dissipation is negligible [Eq. (159)] and where viscous dissipation matters [Eqs. (167) and (175)]. We also find expressions for the temperature at the slipping melt-plate interface in simple shear [Eqs. (157) and (177)]. The plastics engineer can then use these expressions to characterize temperature distributions in slipping flows, which could aid in explaining melt fracture. We expect these results to be accurate when $\text{Pé} \ll 1$.

When slip heating and viscous dissipation are considered together, they do not contribute equally or consistently to the temperature rise experienced by the melt during simple shear or pressure-driven flows. The relative contributions depend on the wall slip speed and shear stress. Temperature rise is attributed to

viscous dissipation when the interfacial shear stress is low or when the exterior surface temperature is low. Slip heating provides most of the heating at high exterior surface temperatures and wall shear stresses. Because both sources of temperature rise are of similar magnitude, neither should be neglected when correcting temperature data in flows where viscous dissipation matters. Additionally, this finding supports slip heating theory by showing its relative importance to viscous dissipation, a common source of temperature rise in polymer melts.

Sections 2.1.5 - 2.1.7, 2.2.3, 3.4 and 3.5 illustrate the usefulness of this work. To test the main results of this work, including the logical consequences of cohesive slip theory, we would undertake a series of die drool measurements (see Sections 7-9 of [15]). We thus propose that the best way to determine the cohesive fracture strength, τ_c, and its possible temperature dependence, is by fitting die drool experimental data.

References

[1] Gilbert, P.H. and A.J. Giacomin, "Slip Heating in Die Drool," Abstracts, The Society of Rheology, 86th Annual Meeting, Philadelphia, PA (October 5-9, 2014), p. 81.

[2] H.S. Carslaw and J.C. Jaeger, Conduction of Heat in Solids, 2nd ed., Oxford University Press, Oxford (1959).

[3] H.S. Carslaw, *Introduction to the mathematical theory of the conduction of heat in solids*, 2nd ed., Completely Revised, MacMillan, London (1921).

[4] S. Middleman, *Fundamentals of polymer processing*, McGraw-Hill, New York (1977).

[5] P.H. Gilbert and A.J. Giacomin, "Slip Heating in Die Drool," *Canadian Journal of Chemical Engineering*, (Accepted: May 2014).

[6] P.H. Gilbert and A.J. Giacomin, "Wall Slip Heating," *Polymer Engineering and Science*, (Accepted: November 2014).

[7] P.H. Gilbert and A.J. Giacomin, "Slip Heating in Die Drool with Viscous Dissipation," *International Polymer Processing*, (Accepted: November 2014).

[8] Ding, F. and A.J. Giacomin, "Die Lines in Plastics Extrusion," *Journal of Polymer Engineering*, **20**(1), 1-39 (2000).

[9] J.D. Gander and A.J. Giacomin, "Review of Die Lip Buildup in Plastics Extrusion," *Polymer Engineering and Science*, **37**(7), 1113-1126 (July, 1997).

[10] J.D. Gander and A.J. Giacomin, "Review of Die Lip Buildup in Plastics Extrusion", S.P.E. Tech. Paper, **XXXXII**, Proc. 54th Annual Tech. Conf. & Exhib., Society of Plastics Engineers, Indianapolis, IN, 1113-1118 (May, 1996).

[11] F. Ding, L. Zhao, A.J. Giacomin and J. D. Gander, "Flaring Dies to Suppress Die Drool," RRC Report No. 166, University of Wisconsin, Madison (October 1999).

[12] J.D. Gander and A.J. Giacomin, "Review of Die Lip Buildup in Plastics Extrusion," RRC Report No. 140, University of Wisconsin, Madison (July 1996).

[13] J. Musil and M. Zatloukal, "Historical review of die drool phenomenon during plastics extrusion," in M. Zatloukal, ed., Novel Trends in Rheology V, *AIP Conference Proceedings*, **1526**, 16-34 (2013).

[14] J.M. Dealy and J. Wang, *Melt rheology and its application in the plastics industry*, 2nd ed., Springer, Dordrecht (2013).

[15] A.M. Schmalzer and A.J. Giacomin, "Die drool theory," *Journal of Polymer Engineering.* **33**, 1-18 (2013).

[16] J. Musil and M. Zatloukal, "Experimental investigation of flow induced molecular weight fractionation during extrusion of HDPE polymer melts," *Chemical Engineering. Science*. **66**, 4814-4823 (2011).

[17] A.M. Schmalzer and A.J. Giacomin, *Die drool and die drool theory*, AIP Conference Proceedings, **1526**, 35-46 (2013).

[18] K.B. Migler, Y. Son, F. Qiao and K. Flynn, "Extensional deformation, cohesive failure, and boundary conditions during sharkskin melt fracture," *Journal of Rheology*. **46**, 383-400 (2002).

[19] K.B. Migler, "Sharkskin instability in extrusion," Chapter 5 in S.G. Hatzikiriakos and K.B. Migler, eds., *Polymer Processing Instabilities: Control and Understanding*, New York: Dekker (2005).

[20] S.G. Hatzikiriakos and K.B. Migler, "Polymer processing additives for melt fracture control," Chapter 2 in M. Kontopoulou, ed., *Applied polymer rheology: Polymeric fluids with industrial applications*, Hoboken, New Jersey: Wiley (2012).

[21] E.C. Achilleos, G. Georgiou, and S.G. Hatzikiriakos "The Role of Processing Aids in the Extrusion of Molten Polymers*," J. Vinyl and Additive Technology*, **8**, 7–24 (2002).

[22] A.M. Schmalzer, "Slip Between Polyolefins and Extrusion Die Surfaces," Masters Thesis, University of Wisconsin, Mechanical Engineering Dept., Madison, WI (June 11, 2013).

[23] S.G. Hatzikiriakos. "Wall slip of molten polymers," *Progress in Polymer Science*, **37**, 624-643 (2012).

[24] R.B. Bird, W.E. Stewart and E.N. Lightfoot, *Transport Phenomena*, Revised 2nd Ed., Wiley & Sons, New York (2007).

[25] R.B. Bird, R.C. Armstrong, and O. Hassager, *Dynamics of polymeric liquids*, vol. 1, 2nd ed., Wiley, New York (1987).

[26] E.E. Rosenbaum, and S.G. Hatzikiriakos, "Wall Slip in the Capillary Flow of Molten Polymers subject to Viscous Heating," *AIChE Journal*, **43**, 598-608 (1997).

[27] A. Yevtushenko and M. Kuciej, "Two calculation schemes for determination of thermal stresses due to frictional heating during braking," *Journal of Theoretical and Applied Mechanics*, **48**, 605-621 (2010).

[28] Gander, J.D., "Die Lip Buildup in Plastics Extrusion," Masters Thesis, University of Wisconsin, Mechanical Engineering Dept., Madison, WI (September, 1997).

[29] D.W. Green and R.H. Perry, *Perry's chemical engineers' handbook*, Eighth Ed. McGraw-Hill, Blacklick, OH (2008).

[30] P.H. Gilbert and A.J. Giacomin, "Slip Heating in Die Drool," PRG Report No. 001, Queen's University, Canada (March 2014).

[31] S.K. Lan and A.J. Giacomin, "Dynamic Slip and Sharkskin Melt Fracture," RRC Report No. 147, University of Wisconsin, Madison (October 1997).

[32] S.K. Lan, "The Role of Dynamic Slip in Extrusion Melt Fracture," Masters Thesis, University of Wisconsin, Mechanical Engineering Dept., Madison, WI (April, 1998).

[33] T. Li, "Rheology of wood-plastics composites," Chapter 6 in M. Kontopoulou, ed., *Applied polymer rheology: Polymeric fluids with industrial applications*, Hoboken, New Jersey: Wiley (2012).

[34] S.G. Hatzikiriakos and J.M. Dealy, "Wall slip of molten high density polyethylene. I. Sliding plate rheometer studies," *Journal of Rheology* **35**(4), 497-523 (1991).

[35] A.M. Schmalzer and A.J. Giacomin, "A new dual-plate slipometer for measuring slip between molten polymers and extrusion die materials," *Review of Scientific Instruments*, **85**, 624-643 (2014).

[36] A.M. Schmalzer and A.J. Giacomin, "Slip Between Polyolefins And Extrusion Die Surfaces," RRC Report No. 205, University of Wisconsin, Madison (May, 2013).

Appendix I: Derivation of Bulk and Drool Temperature Profiles

We begin with the dimensionless time-dependent differential equation for the drool and bulk layers:

$$\frac{\partial\Theta(\xi,\psi)}{\partial\psi}=\frac{\partial^2\Theta(\xi,\psi)}{\partial\xi^2} \tag{179}$$

and perform the Laplace transform with respect to time:

$$s\bar{\Theta}(\xi,s)=\frac{\partial^2\bar{\Theta}(\xi,s)}{\partial\xi^2} \tag{180}$$

Rearranging Eq. (180), we get:

$$\frac{\partial^2\bar{\Theta}(\xi,s)}{\partial\xi^2}-s\bar{\Theta}(\xi,s)=0 \tag{181}$$

which is easily integrated to find:

$$\bar{\Theta}_d(\xi,s)=C_1\cosh\xi\sqrt{s}+C_2\sinh\xi\sqrt{s} \tag{182}$$

for the drool layer, and for the bulk layer:

$$\bar{\Theta}_b(\xi,s)=C_3\cosh\xi\sqrt{s}+C_4\sinh\xi\sqrt{s} \tag{183}$$

We introduce the Laplace transformed dimensionless boundary conditions for the adiabatic mid-plane:

$$\left.\frac{d\bar{\Theta}_b}{d\xi}\right|_{\xi=1}=0 \tag{184}$$

for the heat flux at the slipping interface:

$$\left.\frac{d\bar{\Theta}_d}{d\xi}\right|_{\xi=0}-\left.\frac{d\bar{\Theta}_b}{d\xi}\right|_{\xi=0}=\frac{F}{s} \tag{185}$$

for temperature continuity at the slipping interface:

$$\bar{\Theta}_d(0,s)=\bar{\Theta}_b(0,s) \tag{186}$$

and for the isothermal die wall:

$$\bar{\Theta}_d\left(-a,s\right)=0 \tag{187}$$

Applying Eqs. (184)-(187) to Eqs. (182) and (183), we find the constants C_1, C_2, C_3, and C_4. We first apply Eq. (187) to Eq. (182) to get:

$$\bar{\Theta}_d\left(-a,s\right)=0=C_1\cosh\left(-a\sqrt{s}\right)+C_2\sinh\left(-a\sqrt{s}\right) \tag{188}$$

and rearrange for C_1:

$$C_1=-C_2\tanh\left(-a\sqrt{s}\right) \tag{189}$$

We then combine Eq. (184) with Eq. (183) to get:

$$\left.\frac{\partial\bar{\Theta}_b}{\partial\xi}\right|_{\xi=1}=0=C_4\sqrt{s}\cosh\sqrt{s}+C_3\sqrt{s}\sinh\sqrt{s} \tag{190}$$

where the rightmost expression is the derivative of Eq. (183). Rearranging Eq. (190) yields:

$$C_4=-C_3\tanh\sqrt{s} \tag{191}$$

Inserting the derivatives of Eqs. (182) and (183) into Eq. (185), we find:

$$\left.\frac{\partial\bar{\Theta}_d}{\partial\xi}\right|_{\xi=0}-\left.\frac{\partial\bar{\Theta}_b}{\partial\xi}\right|_{\xi=0}=\frac{F}{s}=C_2\sqrt{s}-C_4\sqrt{s} \tag{192}$$

$$\frac{F}{s^{3/2}}=C_2-C_4 \tag{193}$$

Inserting the derivatives of Eqs. (182) and (183) into Eq. (186), we find:

$$\bar{\Theta}_b\left(0,s\right)=C_3=\bar{\Theta}_d\left(0,s\right)=C_1 \tag{194}$$

$$C_3=C_1 \tag{195}$$

Substituting Eq. (189) into Eq. (191) yields:

$$C_4 = C_2 \tanh\left(-a\sqrt{s}\right)\tanh\sqrt{s} \tag{196}$$

which we insert into Eq. (193) to get:

$$\frac{F}{s^{3/2}} = C_2 + C_2 \tanh\left(a\sqrt{s}\right)\tanh\sqrt{s} \tag{197}$$

$$C_2 = \frac{F}{s^{3/2}\left(1+\tanh\left(a\sqrt{s}\right)\tanh\sqrt{s}\right)} \tag{198}$$

which is used to determine the remaining constants:

$$C_4 = \frac{F\tanh\left(-a\sqrt{s}\right)\tanh\sqrt{s}}{s^{3/2}\left(1+\tanh\left(a\sqrt{s}\right)\tanh\sqrt{s}\right)} \tag{199}$$

$$C_1 = C_3 = -\frac{F\tanh\left(-a\sqrt{s}\right)}{s^{3/2}\left(1+\tanh\left(a\sqrt{s}\right)\tanh\sqrt{s}\right)} \tag{200}$$

Substituting constants for the drool layer temperature profile:

$$\bar{\Theta}_d\left(\xi,s\right) = \frac{F\tanh\left(a\sqrt{s}\right)\cosh\xi\sqrt{s} + F\sinh\xi\sqrt{s}}{s^{3/2}\left(1+\tanh\left(a\sqrt{s}\right)\tanh\sqrt{s}\right)} \tag{201}$$

where the identity for the hyperbolic tangent is:

$$\tanh\left(a\sqrt{s}\right) = \frac{e^{a\sqrt{s}} - e^{-a\sqrt{s}}}{e^{a\sqrt{s}} + e^{-a\sqrt{s}}} \tag{202}$$

Simplifying Eq. (201), we get:

$$\bar{\Theta}_d\left(\xi,s\right) = \frac{F\left(\frac{e^{a\sqrt{s}} - e^{-a\sqrt{s}}}{e^{a\sqrt{s}} + e^{-a\sqrt{s}}}\right)\left(\frac{e^{\xi\sqrt{s}} + e^{-\xi\sqrt{s}}}{2}\right) + F\frac{e^{\xi\sqrt{s}} - e^{-\xi\sqrt{s}}}{2}}{s^{3/2}\left(1+\left(\frac{e^{a\sqrt{s}} - e^{-a\sqrt{s}}}{e^{a\sqrt{s}} + e^{-a\sqrt{s}}}\right)\left(\frac{e^{\sqrt{s}} - e^{-\sqrt{s}}}{e^{\sqrt{s}} + e^{-\sqrt{s}}}\right)\right)} \tag{203}$$

$$\bar{\Theta}_d(\zeta,s)=\frac{F}{2s^{3/2}}\left[\begin{array}{c}\left(e^{a\sqrt{s}}-e^{-a\sqrt{s}}\right)\left(e^{\zeta\sqrt{s}}+e^{-\zeta\sqrt{s}}\right)\left(e^{\sqrt{s}}+e^{-\sqrt{s}}\right)\\ +\left(e^{\zeta\sqrt{s}}-e^{-\zeta\sqrt{s}}\right)\left(e^{a\sqrt{s}}+e^{-a\sqrt{s}}\right)\left(e^{\sqrt{s}}+e^{-\sqrt{s}}\right)\\ \left(e^{a\sqrt{s}}+e^{-a\sqrt{s}}\right)\left(e^{\sqrt{s}}+e^{-\sqrt{s}}\right)\\ +\left(e^{a\sqrt{s}}-e^{-a\sqrt{s}}\right)\left(e^{\sqrt{s}}-e^{-\sqrt{s}}\right)\end{array}\right] \tag{204}$$

$$\bar{\Theta}_d(\zeta,s)=\frac{F}{2s^{3/2}}\left[\frac{e^{(a+\zeta+1)\sqrt{s}}-e^{-(a+\zeta+1)\sqrt{s}}+e^{(a+\zeta-1)\sqrt{s}}-e^{-(a+\zeta-1)\sqrt{s}}}{e^{(a+1)\sqrt{s}}+e^{-(1+a)\sqrt{s}}}\right] \tag{205}$$

$$\bar{\Theta}_d(\zeta,s)=\frac{F}{2s^{3/2}}\left[\frac{\sinh(a+\zeta+1)\sqrt{s}+\sinh(a+\zeta-1)\sqrt{s}}{\cosh(a+1)\sqrt{s}}\right] \tag{206}$$

$$s\bar{\Theta}_d(\zeta,s)=\frac{F}{2s^{1/2}}\left[\frac{\sinh(a+\zeta+1)\sqrt{s}+\sinh(a+\zeta-1)\sqrt{s}}{\cosh(a+1)\sqrt{s}}\right] \tag{207}$$

for the drool layer. Inverting using Heaviside expansion theorem, we obtain:

$$\frac{d\Theta_d(\zeta,\psi)}{d\psi}=L^{-1}\left(\frac{F}{2s^{1/2}}\left[\frac{\sinh(a+\zeta+1)\sqrt{s}+\sinh(a+\zeta-1)\sqrt{s}}{\cosh(a+1)\sqrt{s}}\right]\right) \tag{208}$$

$$Q(s)=\sqrt{s}\cosh(a+1)\sqrt{s} \tag{209}$$

The roots of Eq. (209) are:

$$A_i=0 \tag{210}$$

$$A_i=\sqrt{s_i}=\left(\frac{(2n+1)\pi i}{2(a+1)}\right) \tag{211}$$

Applying the theorem and the roots of the denominator reveals:

$$2P(A)=\sinh(a+\zeta+1)A+\sinh(a+\zeta-1)A \tag{212}$$

$$\frac{P(A)}{Q'(A)}=\frac{\sinh(a+\zeta+1)A+\sinh(a+\zeta-1)A}{\left((a+1)\sinh(a+1)A+\dfrac{\cosh(a+1)A}{A}\right)} \tag{213}$$

$$\frac{P(A)}{Q'(A)}=\frac{\sinh(a+\zeta+1)\left(\frac{(2n+1)\pi i}{2(a+1)}\right)+\sinh(a+\zeta-1)\left(\frac{(2n+1)\pi i}{2(a+1)}\right)}{\left((a+1)\sinh(a+1)\left(\frac{(2n+1)\pi i}{2(a+1)}\right)+\frac{\cosh(a+1)\left(\frac{(2n+1)\pi i}{2(a+1)}\right)}{\left(\frac{(2n+1)\pi i}{2(a+1)}\right)}\right)} \tag{214}$$

The identity for converting hyperbolic functions to trigonometric functions is:

$$\sinh(x)=-i\sin(ix) \tag{215}$$

Apply this identity to Eq. (214) and simplifying yields:

$$\frac{P(A)}{Q'(A)}=\frac{\sin(a+\zeta+1)\left(\frac{(2n+1)\pi}{2(a+1)}\right)+\sin(a+\zeta-1)\left(\frac{(2n+1)\pi}{2(a+1)}\right)}{\left((a+1)\sin(a+1)\left(\frac{(2n+1)\pi}{2(a+1)}\right)\right)} \tag{216}$$

$$\frac{P(A)}{Q'(A)}=\frac{\sin(a+\zeta+1)\left(\frac{(2n+1)\pi}{2(a+1)}\right)+\sin(a+\zeta-1)\left(\frac{(2n+1)\pi}{2(a+1)}\right)}{\left((a+1)(-1)^n\right)} \tag{217}$$

The general solution form is:

$$\frac{d\Theta_d(\zeta,\psi)}{d\psi}=F\sum_{n=0}\frac{P(A)}{Q'(A)}e^{A^2\psi} \tag{218}$$

Substituting Eqs. (217) and (211) into Eq. (218), we find:

$$\frac{d\Theta_d(\zeta,\psi)}{d\psi}=F\sum_{n=0}\frac{\sin(a+\zeta+1)\left(\frac{(2n+1)\pi}{2(a+1)}\right)+\sin(a+\zeta-1)\left(\frac{(2n+1)\pi}{2(a+1)}\right)}{\left((a+1)(-1)^n\right)}e^{-\left(\frac{(2n+1)\pi}{2(a+1)}\right)^2\psi} \tag{219}$$

$$\frac{d\Theta_d(\zeta,\psi)}{d\psi}=\frac{F}{(a+1)}\sum_{n=0}(-1)^n\left(\sin(a+\zeta+1)\lambda+\sin(a+\zeta-1)\lambda\right)e^{-\lambda^2\psi} \tag{220}$$

where:

$$\lambda = \frac{(2n+1)\pi}{2(a+1)} \tag{221}$$

Integrating Eq. (220) produces:

$$\Theta_d(\xi,\psi) = \frac{F}{(a+1)}\sum_{n=0}\frac{(-1)^n}{\lambda^2}\left(\sin(a+\xi+1)\lambda + \sin(a+\xi-1)\lambda\right)\left(1-e^{-\lambda^2\psi}\right) \tag{222}$$

which is the drool layer temperature profile.

Solving for the bulk temperature profile:

$$\bar{\Theta}_b(\xi,s) = C_3\cosh\xi\sqrt{s} + C_4\sinh\xi\sqrt{s} \tag{223}$$

Substitute constants:

$$\bar{\Theta}_b(\xi,s) = -\frac{F\tanh\left(-a\sqrt{s}\right)\cosh\xi\sqrt{s} + F\tanh\left(-a\sqrt{s}\right)\tanh\sqrt{s}\sinh\xi\sqrt{s}}{s^{3/2}\left(1+\tanh\left(a\sqrt{s}\right)\tanh\sqrt{s}\right)} \tag{224}$$

which simplifies to:

$$s\bar{\Theta}_b(\xi,s) = \frac{F}{2s^{1/2}}\left[\frac{\left(e^{a\sqrt{s}}-e^{-a\sqrt{s}}\right)\left(e^{\xi\sqrt{s}}+e^{-\xi\sqrt{s}}\right)\left(e^{\sqrt{s}}+e^{-\sqrt{s}}\right) + \left(e^{-a\sqrt{s}}-e^{a\sqrt{s}}\right)\left(e^{\sqrt{s}}-e^{-\sqrt{s}}\right)\left(e^{\xi\sqrt{s}}-e^{-\xi\sqrt{s}}\right)}{e^{(a+1)\sqrt{s}}+e^{-(1+a)\sqrt{s}}}\right] \tag{225}$$

$$s\bar{\Theta}_b(\xi,s) = \frac{F}{2s^{1/2}}\left[\frac{\left(\begin{array}{l} e^{(a+\xi+1)\sqrt{s}} - e^{(\xi-a+1)\sqrt{s}} + e^{(a-\xi+1)\sqrt{s}} - e^{-(\xi+a+1)\sqrt{s}} \\ +e^{(a+\xi-1)\sqrt{s}} - e^{(\xi-a-1)\sqrt{s}} + e^{(a-\xi-1)\sqrt{s}} - e^{-(\xi+a-1)\sqrt{s}} \end{array}\right) + \left(\begin{array}{l} e^{(\xi-a+1)\sqrt{s}} - e^{(a+\xi+1)\sqrt{s}} + e^{-(\xi+a+1)\sqrt{s}} + e^{(a-\xi+1)\sqrt{s}} \\ -e^{(\xi-a-1)\sqrt{s}} + e^{(a+\xi-1)\sqrt{s}} - e^{-(\xi+a-1)\sqrt{s}} - e^{(a-\xi-1)\sqrt{s}} \end{array}\right)}{e^{(a+1)\sqrt{s}}+e^{-(1+a)\sqrt{s}}}\right] \tag{226}$$

$$s\bar{\Theta}_b(\xi,s) = \frac{F}{2s^{1/2}}\left[\frac{\sinh(a-\xi+1)\sqrt{s} + \sinh(a+\xi-1)\sqrt{s}}{\cosh(a+1)\sqrt{s}}\right] \tag{227}$$

Inverting Eq. (227), we find:

$$\frac{d\Theta_b(\xi,\psi)}{d\psi} = L^{-1}\left(\frac{F}{2s^{1/2}}\left[\frac{\sinh(a-\xi+1)\sqrt{s}+\sinh(a+\xi-1)\sqrt{s}}{\cosh(a+1)\sqrt{s}}\right]\right) \tag{228}$$

with solution form of:

$$\frac{d\Theta_b(\xi,\psi)}{d\psi} = F\sum_{n=0}\frac{P(A)}{Q'(A)}e^{A^2\psi} \tag{229}$$

where:

$$2P(A) = \sinh(a-\xi+1)A+\sinh(a+\xi-1)A \tag{230}$$

and:

$$Q(A^2) = A\cosh(a+1)A \tag{231}$$

The roots of Eq. (231) are:

$$A_i = 0 \tag{232}$$

$$A_i = \sqrt{s_i} = \left(\frac{(2n+1)\pi i}{2(a+1)}\right) \tag{233}$$

The ratio of P to Q′ is:

$$\frac{P(A)}{Q'(A)} = \frac{\sinh(a-\xi+1)A+\sinh(a+\xi-1)A}{\left((a+1)\sinh(a+1)A+\dfrac{\cosh(a+1)A}{A}\right)} \tag{234}$$

Substituting the zeros and converting to trigonometric functions, we obtain:

$$\frac{P(A)}{Q'(A)} = \frac{\sin(a-\xi+1)\left(\dfrac{(2n+1)\pi}{2(a+1)}\right)+\sin(a+\xi-1)\left(\dfrac{(2n+1)\pi}{2(a+1)}\right)}{\left((a+1)\sin(a+1)\left(\dfrac{(2n+1)\pi}{2(a+1)}\right)\right)} \tag{235}$$

Further simplification yields:

$$\frac{P(A)}{Q'(A)} = \frac{\sin(a-\xi+1)\lambda + \sin(a+\xi-1)\lambda}{(a+1)(-1)^n} \tag{236}$$

Substituting into Eq. (229), we find:

$$\frac{d\Theta_b(\xi,\psi)}{d\psi} = F\sum_{n=0}\frac{\sin(a-\xi+1)\lambda + \sin(a+\xi-1)\lambda}{(a+1)(-1)^n} e^{-\left(\frac{(2n+1)\pi}{2(a+1)}\right)^2\psi} \tag{237}$$

Integrating with respect to ψ yields:

$$\Theta_b(\xi,\psi) = \frac{F}{a+1}\sum_{n=0}\frac{(-1)^n}{\lambda^2}\left(\sin(a-\xi+1)\lambda + \sin(a+\xi-1)\lambda\right)\left(1-e^{-\lambda^2\psi}\right) \tag{238}$$

which is the dimensionless bulk layer temperature profile.